UCLouvain

École polytechnique de Louvain

Stochastic Geometry based Optimization of Coverage and Exposure in Wireless Networks

Author: **Julien PIRARD**
Supervisors: **Luc VANDENDORPE, Claude OESTGES**
Readers: **Jérôme LOUVEAUX, Charles WIAME**
Academic year 2020–2021
Master [120] in Electrical Engineering

Acknowledgments

I would like to express my gratitude to my supervisors Prof. Luc Vandendorpe and Prof. Claude Oestges for the advice they provide me during this year.

Thank you in particular to Charles Wiame for his availability and monitoring. He guided throughout this master's thesis.

I also would like to thank Prof. Jérôme Louveaux for agreeing to be a reader of my thesis.

Finally, I would like to thank my parents and friends for their continuous support, and Oriane, Francis, Johanne and Ming for their precious help.

Abstract

This master's thesis aims to introduce a joint analysis of coverage and exposure of sub-6[GHz] downlink transmissions in Heterogeneous Networks (HetNets) using stochastic geometry. This analysis focuses on a joint optimization of coverage and exposure in HetNets. The objective of this optimization is to provide some explanations about how a HetNet should be deployed in order to ensure a given Quality-of-Service and limit the exposure. For this purpose, a performance metric evaluating coverage and exposure, defined as a joint probability, in a HetNet is developed. Based on this metric, two constrained optimization problems on the tier densities and transmission powers are introduced and solved analytically: a general network deployment and a network expansion. Solving these optimizations demonstrates the relation between the network characteristics and its performances, and illustrates the impact of the path-loss on the optimal deployment strategy.

Contents

List of Abbreviations

BS	Base Station
CCDF	Complementary Cumulative Distribution Function
CDF	Cumulative Distribution Function
CF	Characteristic Function
CP	Coverage Probability
DAR	Distance Association Rule
EXPO	Exposure
EP	Exposure Probability
HetNet	Heterogeneous Network
HomNet	Homogeneous Network
HPPP	Homogeneous Poisson Point Process
KTN	K-tiers Network
JPCE	Joint Probability of Coverage and Exposure
LT	Laplace Transform
LTARP	Long-Term Averaged Received Power
MFL	Minimum Fraction Load
MRP	Minimum Received Power
PLE	Path-Loss Exponent
PAR	Power Association Rule

PDF	Probability Density Function
PGFL	Probability Generating Functional
PP	Point Process
PPP	Poisson Point Process
RV	Random Variable
RMS	Root Mean Square
SIR	Signal-To-Noise Ratio
SG	Stochastic Geometry
UE	User Equipment
2TN	2-tiers Network
4G	Fourth Generation
5G	Fifth Generation

Chapter 1

Introduction

The recent deployment of the 5G networks has led to questions about whether the the growing wireless communications poses health risks. This technology requires a lot of new Base Stations (BSs) which fuels concerns about the exposure in mobile networks. Nevertheless, because there are more 5G antennas, each one can transmit at lower power levels than previous 4G. Therefore, their level of radiation should be lower. This network expansion forces us from now to consider the exposure in the study of wireless networks.

To cope with the increasing capacity demand and device populations, cellular networks are no longer single-tiered networks with macro BSs only. Because macro BSs are expensive to deploy in terms of time and money, cellular operators tend to expand their networks via smaller BSs. Modern cellular networks are thus multi-tiered networks that are composed of macro BSs and several types of small BSs, micro, pico and femto [1]. This kind of network is called **Heterogeneous Network** (HetNet). **Macro** BSs fulfill the baseline of coverage in Long-Term Evolution networks. Macrocell antennas are mounted on ground-based masts, rooftops or other existing structures to provide coverage to large area from hundreds of meters to several kilometers [2], [3]. **Micro** BSs have a lower transmission power than Macro BSs. They are used to cover both indoor or outdoor crowed area such as malls, hotels, or a transportation hubs. Micro antennas can also be placed in areas not sufficiently covered by Macro BSs [2], [3]. **Pico** BSs are often deployed for indoor applications, and **Femto** BSs are often self-deployed for small rooms and home requirements [2], [3]. Modern wireless networks can thus be described by their tier features: the density (number of BSs per area unit), the transmission power and also the conditions of wave propagation.

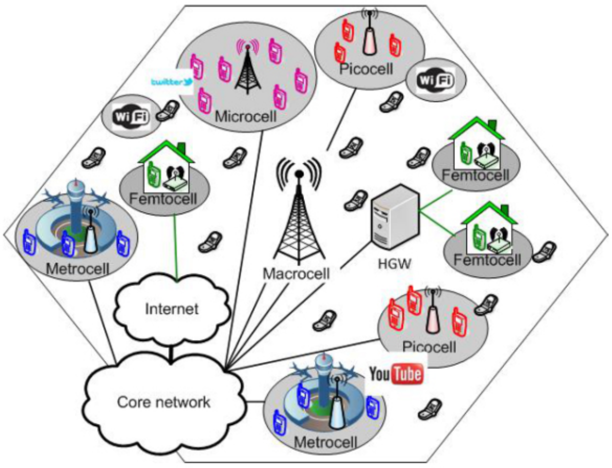

Figure 1.1: Illustration of a HetNet [4]

The purpose of this master's thesis is to introduce a joint analysis of the Quality of Service (QoS) and **exposure** of sub-6[GHz] **downlink** transmissions in a HetNet. In wireless networks, the QoS is usually measured by means of **coverage**. This analysis is focused on two main objectives: the formulation of a **performance metric** combining the coverage and exposure, and the formulation of solvable **joint optimizations** of coverage and exposure. The performance metric is developed using Stochastic Geometry (SG) and is validated with Monte-Carlo (MC) simulations. The joint optimization aims to provide some explanations about how a HetNet should be deployed in order to ensure a given QoS and limit the exposure. Depending on conditions of propagation in the tiers, one should suggest to adapt the features of the HetNet. In this work, based on the optimization problems, the impact of the HetNet densities, transmission powers and the interaction between the tiers is studied. In SG, numerous works (e.g. [5], [6], [7]) already introduce optimization problems for the energy efficiency in HetNets but none combines coverage and exposure.

Stochastic Geometry is the area of mathematical research that is aimed to provide suitable mathematical models and appropriate statistical methods to study and analyse random spatial patterns [8]. Point processes are the most basic and important of such objects. Hence, point process theory is often considered as the main sub-field of SG [8]. In wireless communications, point processes are used to model the spatial locations of nodes such as User Equipment's (UEs) and BSs [8]. SG provides frameworks to evaluate statistical averages of performances in wireless networks.

This master's thesis is structured as follows: in chapter 2, all the mathematical background used in this work is described.

Next, in chapter 3, the mathematical modelling of wireless networks is detailed. This includes the HetNet model, the channel model and the performance metrics defined in this study.

The fourth chapter is dedicated to the development of a SG based theoretical model for the performance metric combining coverage and exposure in HetNets.

Finally, in chapter 5 and 6, two constrained optimization problems are introduced: a joint optimization of coverage and exposure of a HetNet deployment with common conditions of wave propagation and a joint optimization of coverage and exposure of a HetNet expansion.

Chapter 2

Mathematical Background: Stochastic Geometry

This chapter details all the mathematical background on which the frameworks developed in this work are based. All the developments and proofs derived in this work rely on definitions, lemmas, propositions and theorems given in this chapter. This mathematical background is mainly focused on Point Process, and especially Poisson Point Process.

2.1 Law of Total Probability

Let define a sample space S as a union of mutually exclusive subsets $\{B_1, B_2, ..., B_k\}$:

- $S = B_1 \cup B_2 \cup ... \cup B_k$
- $B_i \cap B_j = \emptyset, \quad \forall\, i \neq j$

Then the collection of sets $\{B_1, B_2, ..., B_k\}$ is said to be a partition of S, with $\mathbb{P}(B_i) > 0$, for any $i = 1, 2, ..., k$.
If A is any subset of S, then [9]

$$\mathbb{P}(A) = \sum_{i=1}^{k} \mathbb{P}[A|B_i]\mathbb{P}(B_i)$$

Definition from [9].

2.2 Poisson Law

The **Poisson probability distribution** models the probability distribution of the number Y of rare events that occur in space, time, volume or any other dimension,

where λ is the average value of Y.
A Random Variable (RV) Y is said to have a Poisson probability distribution if and only if the Probability Density Function (PDF) of Y is

$$f_Y(y) = \frac{\lambda^y}{y!} \exp\left(-\lambda\right), \quad y = 0, 1, 2, ..., \lambda > 0.$$

Definition from [9].

2.3 Point Process Theory

2.3.1 General Definition

A **Point Process** (PP) $\mathbf{\Phi}$ is a countable random collection of points that reside in some measure space, usually the Euclidean space $\mathbb{R}^n$ [8]. It can be described by using two formalisms:

- **Random set formalism :** PP is defined as the set of random variables $X_i \subset \mathbb{R}^n$ corresponding to point coordinates [10], [8].
- **Random measure formalism :** PP is characterized by counting the number of points falling in sets $A \subset \mathbb{R}^n$, i.e., $\Phi(A)$. Hence, $\Phi(A)$ is a RV that assumes non-negative integer values. $\Phi(\cdot)$ is called **random counting measure** [8], [10].

  $$\mathbf{\Phi} = \{\mathbf{X}_i, i \in \mathbb{N}\} \quad \Longleftrightarrow \quad \Phi(A) : A \subset \mathbb{R}^n \to \mathbb{N} : A \to \sum_{\mathbf{X}_i \in A} \mathbf{1}(\mathbf{X}_i \in A)$$

PP is usually used to model the spatial locations of network nodes as BSs and UEs. In this work, PPs are defined in a two-dimensional space $\mathbb{R}^2$. Some useful properties and measures can be defined. Let $\mathbf{\Phi}$ be a PP.

Stationary Property: $\mathbf{\Phi}$ is said to be stationary if the translated PP $\mathbf{\Phi}_x = \{\mathbf{X}_i + x, i \in \mathbb{N}\}$ has the same distribution as $\mathbf{\Phi}$ for every $x \in \mathbb{R}^n$ [8].

Void Probability: Its void probability over all bounded sets A is defined as $\mathbb{P}\left[\Phi(A) = 0\right]$ for $A \subset \mathbb{R}^n$ [8].

$$V_{\mathbf{\Phi}} : A \subset \mathbb{R}^n \to \mathbb{R} : A \to \mathbb{P}\left[\Phi(A) = 0\right]$$

Intensity Measure: Its intensity measure $\Lambda_{\mathbf{\Phi}}$ is defined as the mean of the random counting measure [8].

$$\Lambda_{\mathbf{\Phi}} : A \subset \mathbb{R}^n \to \mathbb{R} : A \to \mathbb{E}_{\mathbf{\Phi}}\left[\Phi(A)\right]$$

Exclusion Region: $\mathbf{\Phi}/r$ denotes a new PP defined by the set of points $X_i \subset \mathbb{R}^n$ located at a distance to the origin higher than r .

$$\mathbf{\Phi}/r = \{\mathbf{X}_i, i \in \mathbb{N} | \|\mathbf{X}_i\| > r\}$$

2.3.2 Poisson Point Process

A PP $\mathbf{\Phi}$ of intensity measure $\mathbf{\Lambda}$ is **Poisson Point Process** (PPP) if:

- the number of points in any bounded set $A \subset \mathbb{R}^n$ has a **Poisson distribution** , i.e, [8]
$$\mathbb{P}\left[\Phi(A) = k\right] = \frac{(\Lambda(A))^k}{k!} \exp\left(-\Lambda(A)\right) \tag{2.1}$$
- the number of points in disjoint sets are independent, i.e, for every $A \subset \mathbb{R}^n$ and $B \subset \mathbb{R}^n$ with $A \cap B = \emptyset$, $\Phi(A)$ and $\Phi(B)$ are independent [8].

A PPP is completely characterized by its intensity measure Λ [8]. It can also be defined by its **intensity function** $\lambda : \mathbb{R}^n \rightarrow \mathbb{R}$. The density $\lambda(\mathbf{x})$ of a PPP is defined as the intensity measure for an infinitesimal volume $d\boldsymbol{x} \subset \mathbb{R}^n$ located at position $\boldsymbol{x} \subset \mathbb{R}^n$ [10], [8].

$$\Lambda(d\boldsymbol{x}) = \lambda(\boldsymbol{x})d\boldsymbol{x} \Longleftrightarrow \Lambda(A) = \int_A \lambda(\boldsymbol{x})d\boldsymbol{x}$$

A **Homogeneous Poisson Point Process** (HPPP) is a stationary PPP with a uniform density λ. The intensity measure is then expressed as $\Lambda(A) = \lambda|A|$ for any subset $A \subset \mathbb{R}^n$. Figure 2.1 illustrates an inhomogeneous PPP and a HPPP.

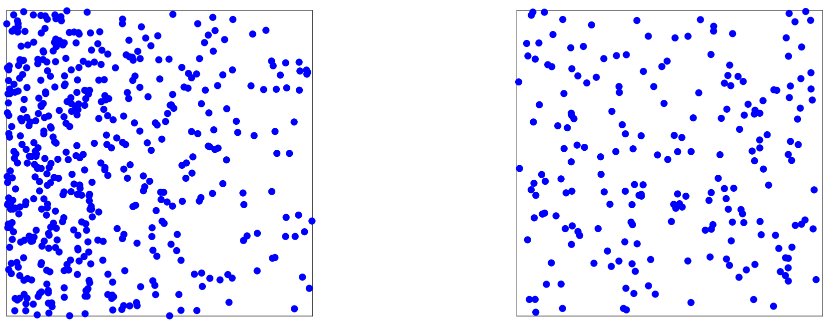

(a) Inhomogeneous PPP (b) Homogeneous PPP

Figure 2.1: Poisson Point Process

PPPs, and particularly HPPPs, are widely used in SG to model wireless networks. The point distribution is realistic compared to node distribution in real wireless networks [10]. Furthermore, PPPs offer useful properties that lead to tractable models.

2.3.3 Poisson Point Process: Useful Properties and Campbell's Theorem

Void Probability of HPPP - Nearest Point Distribution

Let $\mathbf{\Phi} \in \mathbb{R}^2$ be a HPPP of density λ and D the distance of the nearest point of $\mathbf{\Phi}$ to the origin.

Proposition 2.1 (CCDF of the Nearest Point [8])

The Complementary Cumulative Distribution Function (CCDF) of the distance D in $\mathbf{\Phi}$ is given by:

$$CCDF_D(r) = \mathbb{P}\left[D \geq r\right] = \exp\left(-\lambda\pi r^2\right) \tag{2.2}$$

Proof : See Appendix A.2

Proposition 2.2 (PDF of the Nearest Point [8])

The Probability Density Function (PDF) of the distance D in $\mathbf{\Phi}$ is given by:

$$PDF_D(r) = 2\pi\lambda r \exp\left(-\lambda\pi r^2\right) \tag{2.3}$$

Proof : From Proposition 2.1

Campbell's Theorem

Theorem 2.1 (Campbell's Theorem [8])

Let $\mathbf{\Phi}$ be a PPP of intensity function $\lambda(\boldsymbol{x})$ and $f(\boldsymbol{x}) : \mathbb{R}^n \to \mathbb{R}^+$. Then:

$$\mathbb{E}\left[\sum_{\boldsymbol{x}\in\mathbf{\Phi}} f(\boldsymbol{x})\right] = \int_{\mathbb{R}^n} f(\boldsymbol{x})\lambda(\boldsymbol{x})d\boldsymbol{x} \tag{2.4}$$

Proof: see proof in [8]

For a HPPP of density λ, the Campbell's Theorem states:

$$\mathbb{E}\left[\sum_{\boldsymbol{x}\in\mathbf{\Phi}} f(\boldsymbol{x})\right] = \lambda\int_{\mathbb{R}^n} f(\boldsymbol{x})d\boldsymbol{x} \tag{2.5}$$

Probability Generating Functional

Proposition 2.3 (Probability Generating Functional (PGFL) [8])

Let $\mathbf{\Phi}$ be a PPP of intensity function $\lambda(\boldsymbol{x})$ and $f(\boldsymbol{x}) : \mathbb{R}^n \to [0,1]$ be a real value function. Then:

$$\mathbb{E}\left[\prod_{\boldsymbol{x}\in\mathbf{\Phi}} f(\boldsymbol{x})\right] = \exp\left(-\int_{\mathbb{R}^n}(1-f(\boldsymbol{x}))\lambda(\boldsymbol{x})d\boldsymbol{x}\right) \tag{2.6}$$

Proof: see proof in [8]

For a HPPP of density λ, the PGFL gives:

$$\mathbb{E}\left[\prod_{\boldsymbol{x}\in\mathbf{\Phi}} f(\boldsymbol{x})\right] = \exp\left(-\lambda\int_{\mathbb{R}^n}(1-f(\boldsymbol{x}))d\boldsymbol{x}\right) \tag{2.7}$$

Superposition

Let consider K PPPs $\mathbf{\Phi_k} \in \mathbb{R}^n$ characterized by their intensity measure $\mathbf{\Lambda}_k$, for $k = 1, 2, ..., K$. The superposition of these k PPPs generates a new PPP $\mathbf{\Phi} \in \mathbb{R}^n$ of intensity measure given by $\mathbf{\Lambda} = \sum_{k=1}^{K} \mathbf{\Lambda}_k$. The new PPP is denoted $\mathbf{\Phi} = \bigcup_{k=1}^{K} \mathbf{\Phi}_k$ [10].

2.4 Characteristic Function, Laplace Transform and Gil-Pelaez Theorem

Two alternative ways of describing a RV, the **Characteristic Function** (CF) and the **Laplace Transform** (LT), and a useful theorem, the **Gil-Pelaez Theroem**, are defined in this section.

Let X be a RV with the PDF $f_X(x)$.

Definition 2.1 (Characteristic Function [11])

The CF of X is the **complex** function given by:

$$\phi_X(q) = \mathbb{E}_X\left[\exp(jqX)\right] = \int_{-\infty}^{\infty} \exp\left(jqx\right) f_X(x)dx \tag{2.8}$$

Definition 2.2 (Laplace Transform)

The LT of X is the **real positive** function given by:

$$\mathcal{L}_X(s) = \mathbb{E}_X\left[\exp(-sX)\right] = \int_{0}^{\infty} \exp\left(-sx\right) f_X(x)dx \tag{2.9}$$

The **Gil-Pelaez Theorem** enables to compute the CDF of a RV based on its CF.

Theorem 2.2 (Gil-Pelaez Theorem [10])

For an univariate RV X with integrable CF $\phi_X(t)$, the CDF of X is given by:

$$F_X(x) = \mathbb{P}\left[X \leq x\right] = \frac{1}{2} - \frac{1}{\pi}\int_{0}^{\infty} \frac{\mathrm{Im}\left[\phi_x(q)\exp(-jqx)\right]}{q}dq \tag{2.10}$$

2.5 Useful Lemma

The following Lemma defined in [19] is used in chapters 5 and 6 to develop tractable models in SG.

Lemma 2.1 ([19])

Given positive real numbers $\{a_1, ..., a_n\}$ and defining $c_i = \frac{a_i}{\sum_{j=1, j\neq i}^{n} a_j}$, at most m c_i's can be greater than $\frac{1}{m}$ for any positive integer m.

Proof : See Appendix A.1

Chapter 3

Modelling of Wireless Networks - Downlink

In order to evaluate the performances in wireless networks, models expressing the topology of a network and the wave propagation must be defined.

In this chapter, the first sections are dedicated to the HetNet modelling, channel modelling and the association rule in a network. Then, the three performance metrics studied in this work are defined: the **Coverage Probability**, **Exposure Probability** and **Joint Probability of Coverage and Exposure**. Models and performances metrics proposed in this chapter are defined for a **downlink** transmission in sub-6$[GHz]$.

3.1 Network Modelling

In SG, a HetNet is modelled via independent tiers of BSs. In each tier, BS distribution follows a HPPP characterized by a density $\lambda_k[BS/m^2]$ and a transmission power $P_k[W/m^2]$. Hence, a **K-tiers Network** (KTN) $\mathbf{\Phi}$ is modelled by a superposition of K HPPPs:

$$\mathbf{\Phi} = \bigcup_{k=1}^{K} \mathbf{\Phi}_k$$

For simplicity of notation, the HPPP modelling the k^{th}-tier is defined by the set of BS locations $x_{i,k}$ or their distance to the origin $r_{i,k}$:

$$\mathbf{\Phi}_k = \{x_{i,k}, i \in \mathbb{N}\} = \{r_{i,k}, i \in \mathbb{N}\}$$

BSs are ordered according to their distance to the origin. Therefore, $r_{0,k}$ denotes the nearest BS to the origin in the k^{th}-tier.

For the specific case of a single-tier, the network is simply modelled by one HPPP of density λ and transmission power P. This kind of networks is called **Homogeneous Network** (HomNet).

In SG, thanks to the stationary property of HPPPs, the network performances are evaluated for a single **typical user** located at the origin without loss of generality. Figure 3.1 shows an illustration of a 3-tiers network and a typical user (represented by a cross).

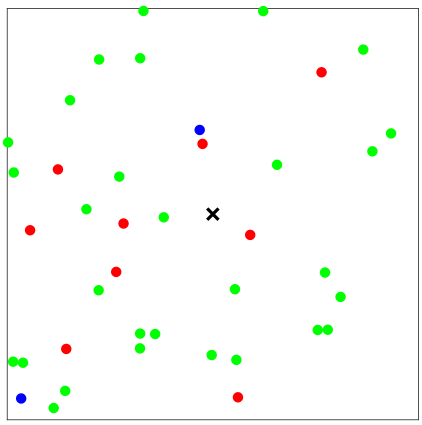

Figure 3.1: HetNet with Typical User

3.2 Channel Modelling

In this section, mathematical models are defined for the wireless communication channels. Usually, three mutually independent, multiplicative propagation phenomena can be distinguished: **Path-Loss**, **Shadowing** and **Multi-Path Fading** [12]. Based on this, the general model of the wireless communication channel used in this work is defined.

3.2.1 Path-Loss

Path-Loss models the attenuation in power density of a electromagnetic wave when it propagates through space [13]. A study in [14] proposes a *Single-Slope Close-In Free Space Reference Distance* model depending on both frequency $f[Hz]$ and distance $r[m]$.

$$PL(f,r)[dB] = 10\alpha \log_{10}\left(\frac{r}{1[m]}\right) + FSPL(f)[dB] \tag{3.1}$$

$$FSPL(f)[dB] = 10\log_{10}(\kappa) \tag{3.2}$$

$$\kappa = \left(\frac{4\pi f}{c}\right)^2 = \left(\frac{4\pi}{\lambda}\right)^2 \tag{3.3}$$

where $c[m/s]$ is the speed of light and $\lambda[m]$, the wavelength. $FSPL(f)$ represents the Free Space Path Loss at a reference distance $1[m]$ and α, the Path-Loss Exponent (PLE). The model proposed in [14] has only one parameter, the PLE, related to the environment. The PLE has typical values in the range of 2 to 4, 2 in free-space and up to 4 for the asymptotic two-ray ground bounce propagation model [14].
A study in [14] shows that a Dual-Slope model fits better with measurements and reduces the RMS error. The *Dual-Slope Close-In Path Loss* model that the authors propose is defined as follows:

$$PL_{\text{dual}}(f,r)[dB] = \begin{cases} FSPL(f)[dB] + 10\alpha_1 \log_{10}(r), & r \le d_{th}, \\ FSPL(f)[dB] + 10\alpha_1 \log_{10}(d_{th}) & \\ +10\alpha_2 \log_{10}\left(\frac{r}{d_{th}}\right), & r > d_{th}. \end{cases} \tag{3.4}$$

where d_{th} denotes the threshold distance, α_1, the PLE for a distance smaller than d_{th} and α_2, the PLE for a distance larger than d_{th}.

3.2.2 Shadowing

Shadowing models fluctuations of the power density due to the presence of obstacles along the propagation path. This phenomenon is expressed by a log-normal RV S modelling variations around the linear path-loss model in log-scale [15].

$$L[dB] = PL[dB] + S, \quad S = 10\log_{10}(s)[dB] \tag{3.5}$$

RV s is said to have a log-normal distribution if $S = 10\log_{10}(s)$ has a normal distribution [9].

$$f_S(s;\mu_S,\sigma_S) = \begin{cases} \frac{10}{s\sigma_S\sqrt{2\pi}\log(10)} \exp\left(-\frac{(10\log_{10}(s)-\mu_S)^2}{2\sigma^2}\right), & s > 0, \\ 0, \quad \text{elsewhere}. \end{cases} \tag{3.6}$$

The mean μ_S is usually set to 0 and the standard deviation σ_S is fitted to the measurements, typically 5 to $12[dB]$ [15].

3.2.3 Multi-Path Fading

Due to the rich diffraction and scattering environment in sub-6$[GHz]$ wireless communications, the signal propagates via multiple paths. Fading is induced by the motion of the transmitter, receiver or scatterers. Consequently, the channel behaves as a stochastic function modelled by a channel gain amplitude RV $|h|$. Three models are commonly used : **Rayleigh**, **Ricean** and **Nakagami-m Fading**.

In this work, the variance of the channel gain amplitude is normalized to the unit which means that the channel does not generate energy.

Rayleigh Fading

Rayleigh fading is suited for environments with rich scattering properties and no dominant path. The channel gain amplitude $|h|$ follows a Rayleigh distribution with parameter σ_h [15].

$$f_{|h|}(h;\sigma_h) = \begin{cases} \frac{h}{\sigma_h^2} \exp\left(-\frac{h^2}{2\sigma_h^2}\right), & h > 0, \\ 0, & \text{elsewhere.} \end{cases} \tag{3.7}$$

The channel power gain $|h|^2$ follows an exponential distribution with parameter $2\sigma_h^2$.

$$f_{|h|^2}(h;2\sigma_h^2) = \begin{cases} \frac{1}{2\sigma_h^2} \exp\left(-\frac{h}{2\sigma_h^2}\right), & h > 0, \\ 0, & \text{elsewhere.} \end{cases} \tag{3.8}$$

The variance of the channel gain amplitude $2\sigma_h^2$ is set to 1 for normalisation, $\mathbb{E}[|h|^2] = 1$. Therefore, σ_h is set to 0.5.

Ricean Fading

Ricean fading occurs when one of the paths, typically the line of sight or a strong reflected signal, is dominant. The channel gain amplitude is Rice distributed with the parameters K and Ω [15].

$$f_{|h|}(h;K,\Omega) = \begin{cases} \frac{2(K+1)h}{\Omega} \exp\left(-K - \frac{(K+1)h^2}{\Omega}\right) I_0\left(2\sqrt{\frac{K(K+1)}{\Omega}}h\right), & h > 0, \\ 0, & \text{elsewhere.} \end{cases} \tag{3.9}$$

K is the ratio between the dominant path ν_h^2 and and the scattered paths $2\sigma_h^2$. Ω is total power of the channel.

$$K = \frac{\nu_h^2}{2\sigma_h^2} \quad \text{and} \quad \Omega = \nu_h^2 + 2\sigma_h^2 \tag{3.10}$$

The PDF of the channel power gain is given by:

$$f_{|h|^2}(h; K, \Omega) = \begin{cases} \frac{(K+1)}{\Omega} \exp\left(-K - \frac{(K+1)h}{\Omega}\right) I_0\left(2\sqrt{\frac{K(K+1)h}{\Omega}}\right), & h > 0, \\ 0, \quad \text{elsewhere.} \end{cases} \tag{3.11}$$

In order to normalize the power of the channel gain, Ω is set to 1.

Nakagami-m Fading

The Nakagami model is very similar to the Ricean channel. However, the PDF of the channel gain amplitude is a closed-form expression, simpler to evaluate than the Ricean model. The channel gain amplitude follows a Nakagami-m distribution with the shape parameter m and spread parameter ω [10].

$$f_{|h|}(h; m, \omega) = \begin{cases} \frac{2m^m h^{2m-1}}{\Gamma(m)\omega^m} \exp\left(-\frac{m}{\omega} h^2\right), & h > 0, \\ 0, \quad \text{elsewhere.} \end{cases} \tag{3.12}$$

The channel power gain follows a Gamma distribution with the shape parameter k and scale parameter θ.

$$f_{|h|^2}(h; k, \theta) = \begin{cases} \frac{h^{k-1}}{\Gamma(k)\theta^m} \exp\left(-\frac{h}{\theta}\right), & h > 0, \\ 0, \quad \text{elsewhere.} \end{cases} \tag{3.13}$$

$$k = m \quad \text{and} \quad \theta = \frac{\omega}{m} \tag{3.14}$$

The variance of the channel gain amplitude $\mathbb{E}\left[|h|^2\right] = \omega$ is set to 1 for normalisation. Therefore, this fading model has one parameter m.

In SG, the channel power gain is usually included in the analysis framework via its CDF, CF or LT. Rayleigh fading is commonly used in sub-6$[GHz]$ for its tractability. Nakagami-m fading is often assumed in mm-Wave networks to model the poor scattering environment [16].

Definition 3.1 (CDF, CF and LT - Rayleigh Fading)

The CDF, CF and LT of the normalized channel power gain modeled by Rayleigh fading are given by:

$$F_{|h|^2}(h) = \exp(-h) \tag{3.15}$$

$$\phi_{|h|^2}(q) = \frac{1}{1 - jq} \tag{3.16}$$

$$\mathcal{L}_{|h|^2}(s) = \frac{1}{1 + s} \tag{3.17}$$

3.2.4 Received Power Modelling

The model of the received power used in this work only combines path-loss, fading and neglects the shadowing for sake of simplicity. A single-slope model is assumed for the path-loss.

Definition 3.2 (Received Power Model)

Let $P_R(r)$ denote the power density received at a distance r from a BS.

$$P_R(r) = \frac{EIRP\kappa^{-1}r^{-\alpha}|h|^2}{4\pi} \quad [W/m^2] \tag{3.18}$$

$EIRP$ denotes the Effective Isotropic Radiated Power of the BS.

$$EIRP = P_T G_T \quad [W] \tag{3.19}$$

where P_T is the BS transmission power and G_T, the antenna gain at the transmission.

The factor $\frac{1}{4\pi}$ is used to express the received power in terms of power density $[W/m^2]$. In the next sections and chapters, EIRP is denoted by P.

3.3 Association Rule

An open access is assumed in this work, which means that the typical user can be served by any BSs. The typical user chooses to associate with the strongest BS in terms of **Long-Term Averaged Received Power** (LTARP). As the fading is averaged out, the expression of the LTARP does not include the fading. As a reminder, the expectation of the normalized channel power gain is 1, $\mathbb{E}\left[|h|^2\right] = 1$.

Definition 3.3 (LTARP)

The LTARP from a BS located at a distance r to the origin is given by:

$$P_{R,AV}(r) = \frac{P\kappa^{-1}r^{-\alpha}}{4\pi} \tag{3.20}$$

The association rule is therefore based on a **Distance Association Rule** (DAR). In the general case of a HetNet, the typical user is associated with the tier providing the highest LTARP.

Definition 3.4 (Distance Association Rule)

Let n denote the index of the tier serving the typical user and $P_{R,AV,k}(r_{0,k})$ the LTARP from the nearest BS to the origin in the k^{th}-tier. For a KTN,

$$n = \text{argmax}_{k\in\{1,\ldots,K\}} P_{R,AV,k}(r_{0,k}) \tag{3.21}$$

In the specific case of a HomNet, the DAR means that the typical user is served by the nearest BS to the origin.

3.4 Performance Metrics

In SG, different metrics are defined depending on the performances evaluated in the network. Due to the spatial randomness of HPPPs and the randomness of the channel model, these metrics are RVs.

The performance metrics studied in this work are related to the **Signal-To-Interference Ratio** (SIR) and the **Exposure** (EXPO). Based on these common metrics, the **Coverage Probability**, **Exposure Probability** and **Joint Probability of Coverage and Exposure** are defined.

Let $\mathcal{S}$ denote the **Useful Signal Power** and $\mathcal{I}$, the **Interfering Signal Power** received by the typical user. In SG, the coverage is usually estimated based on the Signal-to-Interference-plus-Noise Ratio:

$$\mathrm{SINR} = \frac{\mathcal{S}}{\sigma^2 + \mathcal{I}} \tag{3.22}$$

where σ^2 denotes the noise power at the receiver. In this work, the analyses focus on interference limited networks, i.e, by neglecting the noise power. The Signal-to-Interference Ratio is then defined as follows:

$$\mathrm{SIR} = \frac{\mathcal{S}}{\mathcal{I}} \tag{3.23}$$

The Exposure is the total power received by the typical user from all the BSs:

$$\mathrm{EXPO} = \mathcal{S} + \mathcal{I} \tag{3.24}$$

3.4.1 Coverage Probability

A user is said in coverage if he experiences a SIR higher than a given threshold θ. The Coverage Probability (CP) is defined as the probability that the SIR at the typical user location is higher than a given SIR threshold θ.

Definition 3.5 (Coverage Probability)

The CP is defined as follows:

$$\mathbb{P}_{\mathrm{cv}}(\theta) = \mathbb{P}\left[\mathrm{SIR} > \theta\right] \tag{3.25}$$

3.4.2 Exposure Probability

The Exposure Probability (EP) is defined as the probability that the EXPO at the typical user location is lower than a given exposure threshold θ'.

Definition 3.6 (Exposure Probability)

The EP is defined as follows:

$$\mathbb{P}_{\mathrm{expo}}(\theta') = \mathbb{P}\left[\mathrm{EXPO} < \theta'\right] \tag{3.26}$$

The measure unit of the exposure in a wireless network is expressed in $[V/m]$ and the unit of EXPO is $[W/m^2]$. It is then necessary to convert the exposure norm $[V/m]$ in $[W/m^2]$. Let θ'_V denote the exposure norm in $[V/m]$. The exposure threshold θ' is defined as follows:

$$\theta' = \frac{{\theta'_V}^2}{Z} \quad [W/m^2] \tag{3.27}$$

where Z denotes the air impedance, $376.73[\Omega]$.

For information purposes, in Brussels, the total electromagnetic field cannot exceed $6[V/m]$ (at a reference frequency of 900[MHz]) at any time, and in any area accessible to the public. In Wallonia, a decree limits the electromagnetic field to $3[V/m]$ by antenna [17].

3.4.3 Joint Probability of Coverage and Exposure

This performance metric combines both coverage and exposure in a wireless network. The Joint Probability of Coverage and Exposure (JPCE) is defined as the probability that the coverage at the typical user location is higher than a given SIR threshold θ and the exposure is lower than a given exposure threshold θ'.

Definition 3.7 (Joint Probability of Coverage and Exposure)

The JPCE is defined as follows:

$$\begin{aligned} \mathbb{F}(\theta, \theta') &= \mathbb{P}\left[\text{SIR} > \theta, \text{EXPO} < \theta'\right] \\ &= \mathbb{P}\left[\frac{\mathcal{S}}{\mathcal{I}} > \theta, \mathcal{S} + \mathcal{I} < \theta'\right] \end{aligned} \tag{3.28}$$

3.5 Typical Values of Transmission Powers

Table 3.1 provides typical values of BS transmission powers, antenna gains and EIRPs for bands between 1 and $3[GHz]$. The BSs are differentiated according to the type of environments where they are deployed and their tier.

	Macro Rural	**Macro Suburban**	**Macro Urban**	**Micro Urban**	**Small Cell Indoor**
Maximum BS output power $[dBm]$	46	46	46	35	24
Maximum BS antenna gain $[dBi]$	18	16	16	5	0
Maximum BS EIRP $[dBm]$	61	59	59	40	24

Table 3.1: BS characteristics: Transmission Powers (Bandwidth = $20[MHz]$) [18]

Chapter 4

General Framework for the Analysis of Coverage and Exposure of Heterogeneous Networks

In this chapter, a general framework for the coverage and exposure analysis of HetNets is developed. Based on the Gil-Pelaez theorem, a mathematical model is derived for the JPCE. The expression of the performance metric $\mathbb{F}(\theta, \theta')$ is accurate down to sufficiently high thresholds θ'. For too small values of θ', the joint probability is null and the Gil-Pelaez based model assumes negative probabilities. To be computed, the JPCE requires numerical integrations.

In the first instance, the JPCE is developed for a HomNet and general fading. The analysis is then extended to a KTN. Specific models are also derived for Rayleigh fading. These results combine the Gil-Pelaez based model and expressions of the CP developed in [20] for Rayleigh fading. Finally, the model accuracy is evaluated with numerical results obtained by MC simulations for Rayleigh fading.

4.1 Homogeneous Network - General Fading

In a HomNet, the position of BSs is modelled by a HPPP $\mathbf{\Phi}$ with density λ. Every BS uses the same transmission power P. The useful signal and interfering signal experience the same path-loss.

Useful Signal and Interfering Signal

With a DAR, the serving BS in a HomNet is the nearest to the origin. r_0 denotes the distance from the nearest BS to the origin. All the BSs located at a distance larger than r_0 are then considered as interfering BSs. This association rule allows to define an interference boundary $r_{\mathcal{I}}$. The definition of the useful signal and interfering signal is therefore straightforward.

Definition 4.1 (Useful Signal and Interfering Signal - HomNet)

The interference boundary is given by:

$$r_{\mathcal{I}} = r_0 \tag{4.1}$$

The useful signal is given by:

$$\mathcal{S} = \frac{P|h|^2\kappa^{-1}r_0^{-\alpha}}{4\pi} \tag{4.2}$$

The interfering signal is given by:

$$\mathcal{I} = \sum_{r_i \in \mathbf{\Phi}/r_{\mathcal{I}}} \frac{P|h|^2\kappa^{-1}r_i^{-\alpha}}{4\pi} \tag{4.3}$$

For simplicity of notation, the parameter κ and factor $\frac{1}{4\pi}$ are omitted in the developments. One can observe that these parameters simplify in the SIR expression.

$$\text{SIR} = \frac{P|h|^2 r_0^{-\alpha}}{\sum_{r_i \in \mathbf{\Phi}/r_{\mathcal{I}}} P|h|^2 r_i^{-\alpha}}$$

It is also the case for the power P. However, this simplification does not apply to a HetNet. Concerning the exposure, it is assumed that these parameters are included in the threshold θ'.

$$\text{EXPO} = P|h|^2 r_0^{-\alpha} + \sum_{r_i \in \mathbf{\Phi}/r_{\mathcal{I}}} P|h|^2 r_i^{-\alpha} < \frac{\theta' 4\pi}{\kappa^{-1}}$$

With a slight abuse of notation, the quantity $\frac{\theta' 4\pi}{\kappa^{-1}}$ is abbreviated as θ' for the rest of this work.

Serving Distance Statistical Distribution

Since the BSs are deployed in a HPPP, the **serving distance** R_0 is a RV described by its PDF or CCDF obtained from Proposition 2.2 and 2.1.

Proposition 4.1 (PDF and CCDF of R_0 - HomNet)

The PDF $f_{R_0}(r)$ of the serving distance R_0 between the typical user and its serving BS is given by [1]:

$$f_{R_0}(r) = 2\pi\lambda r \exp\left(-\pi\lambda r^2\right), \quad r > 0 \tag{4.4}$$

The CCDF of the serving distance R_0 between the typical user and its serving BS is given by:

$$CCDF_{R_0}(r) = \exp\left(-\pi\lambda r^2\right), \quad r > 0 \tag{4.5}$$

Joint Probability of Coverage and Exposure - Fixed Serving Distance

Let express the JPCE for a fixed serving distance by applying the Gil-Pelaez theorem. The result is derived with respect to the useful signal and interfering signal CFs which are both expressed in terms of the channel power gain CF.

Proposition 4.2 (Useful Signal CF - HomNet)

The useful signal CF for a fixed serving distance r_0 is given by:

$$\phi_{\mathcal{S}}(q; r_0) = \phi_{|h|^2}\left(qPr_0^{-\alpha}\right) \tag{4.6}$$

Proof : see Appendix A.2

Proposition 4.3 (Interfering Signal CF - HomNet)

The interfering signal CF for a fixed serving distance r_0 is given by:

$$\phi_{\mathcal{I}}(q;r_0) = \exp\left(-2\pi\lambda \int_{r_0}^{\infty} \left(1 - \phi_{|h|^2}\left(qPr^{-\alpha}\right)\right) rdr\right) \tag{4.7}$$

Proof : see Appendix A.2

Proposition 4.4 ($\mathbb{F}(\theta,\theta';r_0)$, $\mathbb{P}_{\mathbf{cv}}(\theta;r_0)$, $\mathbb{P}_{\mathbf{expo}}(\theta';r_0)$ - HomNet)

The JPCE for a fixed serving distance r_0 is given by:

$$\begin{aligned} \mathbb{F}(\theta,\theta';r_0) = & \frac{1}{\pi}\int_0^\infty \frac{1}{q}\mathrm{Im}\left[\phi_{\mathcal{S}}(q;r_0)\phi_{\mathcal{I}}(-q\theta;r_0)\right]dq \\ & - \frac{1}{\pi}\int_0^\infty \frac{1}{q}\mathrm{Im}\left[\phi_{\mathcal{S}}(q;r_0)\phi_{\mathcal{I}}(q;r_0)\exp\left(-jq\theta'\right)\right]dq \end{aligned} \tag{4.8}$$

The joint probability can also be expressed with respect to the CP and the EP.

$$\mathbb{F}(\theta,\theta';r_0) = \mathbb{P}\left[\mathrm{SIR} > \theta\right]_{r_0} - \mathbb{P}\left[\mathrm{EXPO} > \theta'\right]_{r_0}$$

The CP and EP for a fixed serving distance r_0 are given by:

$$\mathbb{P}_{\mathrm{cv}}(\theta;r_0) = \frac{1}{2} + \frac{1}{\pi}\int_0^\infty \frac{1}{q}\mathrm{Im}\left[\phi_{\mathcal{S}}(q;r_0)\phi_{\mathcal{I}}(-q\theta;r_0)\right]dq \tag{4.9}$$

$$\mathbb{P}_{\mathrm{expo}}(\theta';r_0) = \frac{1}{2} - \frac{1}{\pi}\int_0^\infty \frac{1}{q}\mathrm{Im}\left[\phi_{\mathcal{S}}(q;r_0)\phi_{\mathcal{I}}(q;r_0)\exp\left(-jq\theta'\right)\right]dq \tag{4.10}$$

Proof : see Appendix A.2

Joint Probability of Coverage and Exposure - Final Expression

To obtain the final expression of the joint probability, $\mathbb{F}(\theta,\theta';r_0)$ is averaged over the RV R_0.

Proposition 4.5 (JPCE, CP, EP - HomNet)

The JPCE is given by:

$$\begin{aligned}\mathbb{F}(\theta, \theta') &= \mathbb{E}_{R_0}\left[\mathbb{F}(\theta, \theta'; r_0)\right] \\ &= \int_0^\infty \mathbb{F}(\theta, \theta'; r_0) f_{R_0}(r_0) dr_0\end{aligned} \tag{4.11}$$

From the linearity of the expectation operator, the joint probability can also be expressed with respect to the CP and the EP.

$$\mathbb{F}(\theta, \theta') = \mathbb{P}_{\text{cv}}(\theta) + \mathbb{P}_{\text{expo}}(\theta') - 1 \tag{4.12}$$

$$\mathbb{P}_{\text{cv}}(\theta) = \mathbb{E}_{R_0}\left[\mathbb{P}_{\text{cv}}(\theta; r_0)\right] \tag{4.13}$$

$$\mathbb{P}_{\text{expo}}(\theta') = \mathbb{E}_{R_0}\left[\mathbb{P}_{\text{expo}}(\theta'; r_0)\right] \tag{4.14}$$

4.2 Heterogeneous Network - General Fading

As a reminder of a KTN modelling, the position of the BSs in each tier is modelled by a HPPP $\mathbf{\Phi}_k$ of density λ_k and characterized by its own transmission power P_k. A general approach is proposed with different path-loss for each tier. Many studies (e.g.[1], [20]) on HetNets in SG use a model in which each tier is characterized by its own PLE α_k.

Useful Signal and Interfering Signal

The useful signal and interfering signals are defined assuming the typical user is served by the k^{th}-tier. Therefore, the serving distance is denoted by $r_{0,k}$. Depending on the transmission powers and PLEs, different interference boundaries are defined for each tier.

Definition 4.2 (Useful Signal and Interfering Signal - HetNet)

Assuming a KTN and based on the DAR, the typical user is served by the k^{th}-tier if:

$$P_k r_{0,k}^{-\alpha_k} > P_i r_{0,i}^{-\alpha_i} \quad \forall i \in \{1, ..., K\}, \quad i \neq k \tag{4.15}$$

The interference boundary of each tier is given by:

$$r_{\mathcal{I}_i} = \left(\frac{P_i r_{0,k}^{\alpha_k}}{P_k} \right)^{1/\alpha_i} \qquad \forall i \in \{1, ..., K\} \tag{4.16}$$

The useful signal is given by:

$$\mathcal{S} = P_k |h|^2 r_{0,k}^{-\alpha_k} \tag{4.17}$$

The interfering signal is given by:

$$\mathcal{I} = \sum_{i=1}^{K} \sum_{r_{j,i} \in \mathbf{\Phi_i} / r_{\mathcal{I}_i}} P_i |h|^2 r_{j,i}^{-\alpha_i} \tag{4.18}$$

Serving Distance Statistical Distribution

The association rule expressed by (4.15), the tier densities, transmission powers and PLEs determine the **Per-Tier Association Probability** and the PDF of the serving distance RV $R_{0,k}$.

Proposition 4.6 (Per-Tier Association Probability)

The probability that the typical user is served by the k^{th}-tier is given by [20]:

$$\mathcal{A}_k = 2\pi\lambda_k \int_0^\infty r \exp\left(-\pi \sum_{i=1}^{K} \lambda_i \left(\frac{P_i}{P_k} \right)^{2/\alpha_i} r^{2\alpha_k/\alpha_i} \right) dr \tag{4.19}$$

If $\{\alpha_i\} = \alpha$ for all $i \in \{1, ..., K\}$, then this gives:

$$\mathcal{A}_k = \frac{\lambda_k}{\sum_{i=1}^{K} \lambda_i P_i^{2/\alpha}} \tag{4.20}$$

Proof : see Appendix A.2

Proposition 4.7 (PDF of $R_{0,k}$)

The PDF $f_{R_{0,k}}(r)$ of the serving distance $R_{0,k}$ between the typical user and its serving BS is given by [1],[20]:

$$f_{R_{0,k}}(r) = \frac{2\pi\lambda_k}{\mathcal{A}_k} r \exp\left(-\pi \sum_{i=1}^{K} \lambda_i \left(\frac{P_i}{P_k}\right)^{2/\alpha_i} r^{2\alpha_k/\alpha_i}\right), \quad r > 0 \tag{4.21}$$

Proof : see Appendix A.2

Joint Probability of Coverage and Exposure - Fixed Serving Distance

Let express the JPCE assuming the typical user is served by the k^{th}-tier and for a fixed serving distance $r_{0,k}$. As for a HomNet, the result is derived with respect to the useful signal and interfering signal CFs.

Proposition 4.8 (Useful Signal CF - HetNet)

Assuming the typical user is served by the k^{th}-tier and for a fixed serving distance $r_{0,k}$, the useful signal CF is given by:

$$\phi_{\mathcal{S}}(q; k, r_{0,k}) = \phi_{|h|^2}\left(qP_k r_{0,k}^{-\alpha_k}\right) \tag{4.22}$$

Proposition 4.9 (Interfering Signal CF - HetNet)

Assuming the typical user is served by the k^{th}-tier and for a fixed serving distance $r_{0,k}$, the interfering signal CF is given by [1]:

$$\phi_{\mathcal{I}}(q; k, r_{0,k}) = \prod_{i=1}^{K} \phi_{\mathcal{I}_i}(q; k, r_{0,k}) \tag{4.23}$$

$$\phi_{\mathcal{I}_i}(q; k, r_{0,k}) = \exp\left(-2\pi\lambda_i \int_{r_{\mathcal{I}_i}}^{\infty} \left(1 - \phi_{|h|^2}\left(qP_i r^{-\alpha_i}\right)\right) r dr\right) \tag{4.24}$$

Proof : see Appendix A.2

Proposition 4.10 ($\mathbb{F}_k(\theta, \theta'; k, r_{0,k})$, $\mathbb{P}_{\mathbf{cv},k}$, $\mathbb{P}_{\mathbf{expo},k}(\theta'; r_{0,k})$ - HetNet)

From Proposition 4.4, assuming the typical user is served by the k^{th}-tier and for a fixed serving distance $r_{0,k}$, the JPCE, CP and EP are given by:

$$\begin{aligned}\mathbb{F}_k(\theta, \theta'; k, r_{0,k}) = &\frac{1}{\pi}\int_0^\infty \frac{1}{q}\mathrm{Im}\left[\phi_{\mathcal{S}}(q; k, r_{0,k})\phi_{\mathcal{I}}(-q\theta; k, r_{0,k})\right] dq \\ &- \frac{1}{\pi}\int_0^\infty \frac{1}{q}\mathrm{Im}\left[\phi_{\mathcal{S}}(q; k, r_{0,k})\phi_{\mathcal{I}}(q; k, r_{0,k}) \exp\left(-jq\theta'\right)\right] dq\end{aligned} \tag{4.25}$$

$$\mathbb{P}_{\mathrm{cv},k}(\theta; k, r_{0,k}) = \frac{1}{2} + \frac{1}{\pi}\int_0^\infty \frac{1}{q}\mathrm{Im}\left[\phi_{\mathcal{S}}(q; k, r_{0,k})\phi_{\mathcal{I}}(-q\theta; k, r_{0,k})\right] dq \tag{4.26}$$

$$\mathbb{P}_{\mathrm{expo},k}(\theta'; k, r_{0,k}) = \frac{1}{2} - \frac{1}{\pi}\int_0^\infty \frac{1}{q}\mathrm{Im}\left[\phi_{\mathcal{S}}(q; k, r_{0,k})\phi_{\mathcal{I}}(q; k, r_{0,k}) \exp\left(-jq\theta'\right)\right] dq \tag{4.27}$$

Joint Probability of Coverage and Exposure - Final Expression

From the law of total probability and by averaging out the serving distance RVs, the final expression of the JPCE in a HetNet can be derived.

Proposition 4.11 (JPCE, CP, EP - HetNet)

The JPCE is given by:

$$\begin{aligned}\mathbb{F}(\theta,\theta') &= \sum_{k=1}^{K}\mathcal{A}_k\mathbb{E}_{R_{0,k}}\left[\mathbb{F}_k(\theta,\theta';k,r_{0,k})\right]\\ &= \sum_{k=1}^{K}\int_0^{\infty}2\pi\lambda_k r_{0,k}\exp\left(-\pi\sum_{i=1}^{K}\lambda_i\left(\frac{P_i}{P_k}\right)^{2/\alpha_j}r_{0,k}^{2\alpha_k/\alpha_j}\right)\\ &\qquad \mathbb{F}_k(\theta,\theta';k,r_{0,k})dr_{0,k}\end{aligned} \tag{4.28}$$

From the linearity of the expectation operator, the joint probability can be expressed with respect to the CP and the EP.

$$\mathbb{F}(\theta,\theta') = \mathbb{P}_{\mathrm{cv}}(\theta) + \mathbb{P}_{\mathrm{expo}}(\theta') - 1 \tag{4.29}$$

$$\mathbb{P}_{\mathrm{cv}}(\theta) = \sum_{k=1}^{K}\mathcal{A}_k\mathbb{E}_{R_{0,k}}\left[\mathbb{P}_{\mathrm{cv},k}(\theta;k,r_{0,k})\right] \tag{4.30}$$

$$\mathbb{P}_{\mathrm{expo}}(\theta') = \sum_{k=1}^{K}\mathcal{A}_k\mathbb{E}_{R_{0,k}}\left[\mathbb{P}_{\mathrm{expo},k}(\theta';k,r_{0,k})\right] \tag{4.31}$$

One can observe that the per-tier association probabilities $\mathcal{A}_k$ simplifiy in the final expression. Therefore, for a HetNet, the general performance metric is obtained by summing the joint probability of each tier. This result comes from the mutual independence between the HPPPs.

4.3 Special Case: Rayleigh Fading

For the special case of Rayleigh fading, closed-form expressions of the useful signal and interfering signal CFs can be derived.

Proposition 4.12 (Useful Signal CF - Rayleigh Fading)

Assuming Rayleigh fading, the useful signal CF is given by:
for a HomNet,

$$\phi_{\mathcal{S}}(q; r_0) = \frac{1}{1 - jqPr_0^{-\alpha}} \tag{4.32}$$

for a HetNet,

$$\phi_{\mathcal{S}}(q; k, r_{0,k}) = \frac{1}{1 - jqP_k r_{0,k}^{-\alpha_k}} \tag{4.33}$$

Proof : from Proposition 4.2 and Definition 3.1

Proposition 4.13 (Interfering Signal CF - Rayleigh Fading)

Assuming Rayleigh fading, the interfering signal CF is given by:
for a HomNet,

$$\phi_{\mathcal{I}}(q; r_0) = \exp\left(\frac{jq2\pi\lambda P r_0^{2-\alpha}}{\alpha - 2}\, {}_2F_1\left(1, 1 - \frac{2}{\alpha}; 2 - \frac{2}{\alpha}; \frac{jq}{Pr_0^{\alpha}}\right)\right) \tag{4.34}$$

for a HetNet,

$$\phi_{\mathcal{I}_i}(q; k, r_{0,k}) = \exp\left(\frac{jq2\pi\lambda_i P_i r_{\mathcal{I}_i}^{2-\alpha_i}}{\alpha_i - 2}\, {}_2F_1\left(1, 1 - \frac{2}{\alpha_i}; 2 - \frac{2}{\alpha_i}; \frac{jq}{P_i r_{\mathcal{I}_i}^{\alpha_i}}\right)\right) \tag{4.35}$$

where ${}_2F_1(\cdot)$ is the Gauss Hypergeometric function.

Proof : see Appendix A.2

By inserting these equations into (4.11) or (4.28), the computation of the JPCE is obtained by a double numerical integration.

Proposition 4.4 shows that the joint probability is a summation of two terms, the CP and a second related to the EP. For Rayleigh fading, a study in [20] proposes a more tractable expression for the CP than the Gil-Pelaez based model. By using the result of this study, the mathematical complexity of the joint probability expression can be reduced.

Proposition 4.14 (Coverage Probability - Rayleigh Fading)

Assuming Rayleigh fading, the CP is given by [20]:
for a HomNet,

$$\mathbb{P}_{\text{cv}}(\theta) = \frac{1}{1 + \mathcal{Z}(\theta, \alpha)} \tag{4.36}$$

for a HetNet,

$$\mathbb{P}_{\text{cv}}(\theta) = \sum_{k=1}^{K} 2\pi\lambda_k \int_0^\infty r \exp\left(-\pi \sum_{j=1}^{K} C_j r^{2\alpha_k/\alpha_j}\right) dr \tag{4.37}$$

If $\{\alpha_i\} = \alpha$ for all $i \in \{1, ..., K\}$, then this gives:

$$\mathbb{P}_{\text{cv}}(\theta) = \frac{1}{1 + \mathcal{Z}(\theta, \alpha)} \tag{4.38}$$

$$\text{where} \quad \mathcal{Z}(\theta, \alpha) = \frac{2\theta}{\alpha - 2} \, {}_2F_1\left(1, 1 - \frac{2}{\alpha}; 2 - \frac{2}{\alpha}; -\theta\right)$$

$$\text{and} \quad C_j = \lambda_j \left(\frac{P_j}{P_k}\right)^{\frac{2}{\alpha_j}} \mathcal{Z}(\theta, \alpha_j)$$

Proof : see proof in [20]

By substituting these equations into expressions (4.12) and (4.29), the joint probability can be computed with a single numerical integration for the CP and a double numerical integration (Gil-Pelaez based model) for the EP.

From equations (4.36) and (4.38), one can observe that the CP is independent from the tier densities and transmission powers for Rayleigh fading. This result is specific to an interference-limited network and to a common PLE. The intuition behind this observation is that change in the densities leads to a change in the useful signal and interfering signal powers with the same factor [19]. A similar reasoning also applies to the transmission powers.

4.4 Numerical Results - Accuracy of the Model

In this section, the accuracy of the Gil-Pelaez based model is evaluated for Rayleigh fading. In order to compute the CP, equations (4.36) and (4.37) from Proposition

4.14 are used. A comparison between SG and MC simulations is provided for a HomNet and a 2-tiers Network (2TN).

4.4.1 Homogeneous Network

Figures 4.1 and 4.2 compare the CP obtained by equation (4.36) and the EP obtained by equation (4.14) with numerical results. One can deduce that both models are accurate. The analytical curves are remarkably close to the simulated curves for all considered thresholds. The validation of the CP expression is already done in [20].

Figure 4.3 shows the JPCE obtained by MC simulations (a), by SG (b) and the absolute observed error (c). As mentioned previously, the joint probability is the subtraction of the CP and the CCDF of the exposure. Therefore, for small thresholds θ' (that depend on SIR threshold θ) the expression can assume negative values. In Figure (b), the joint probability is then truncated to positive values only. One can observe that the expression is negative when the real probability (Figure (a)) is null. This truncation induces an edge effect as shown in Figure (c). For thresholds θ' sufficiently high, the model has an accuracy about one thousandth.

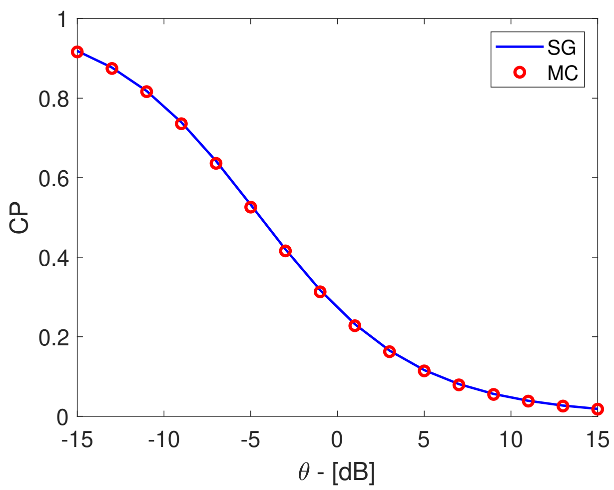

Figure 4.1: CP - HomNet : $\lambda = 10^{-6}[BS/m^2]$, $P = 30[dBm]$, $\alpha = 2.5$.

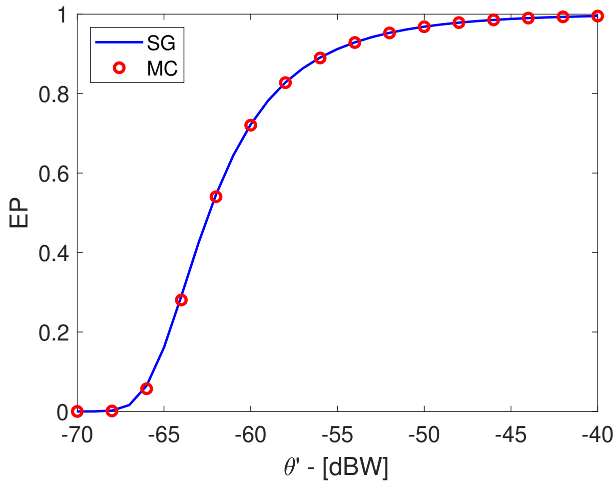

Figure 4.2: EP - HomNet : $\lambda = 10^{-6}[BS/m^2]$, $P = 30[dBm]$, $\alpha = 2.5$.

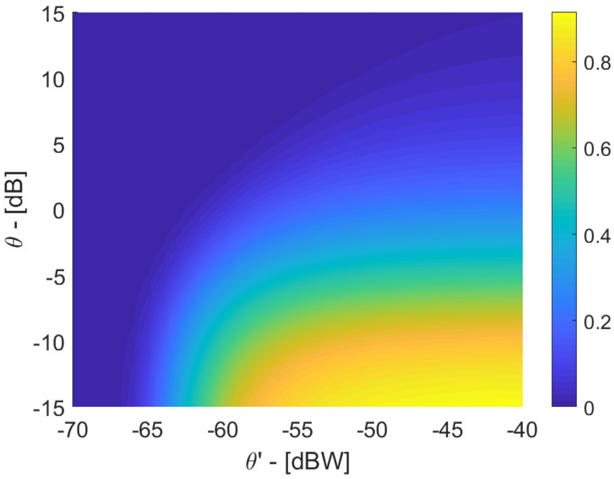

(a) Monte-Carlo Simulations

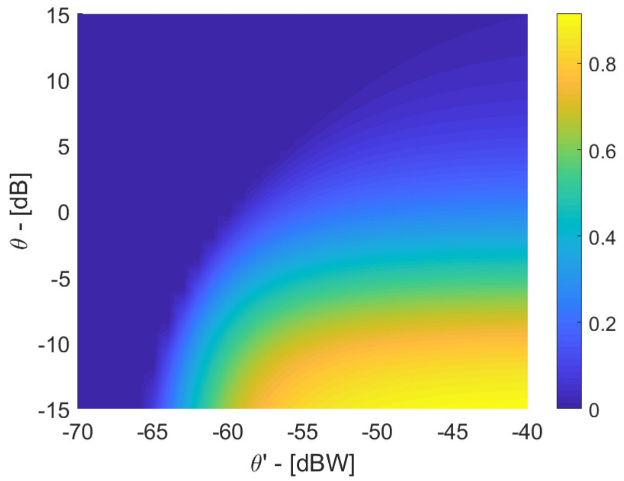

(b) Stochastic Geometry

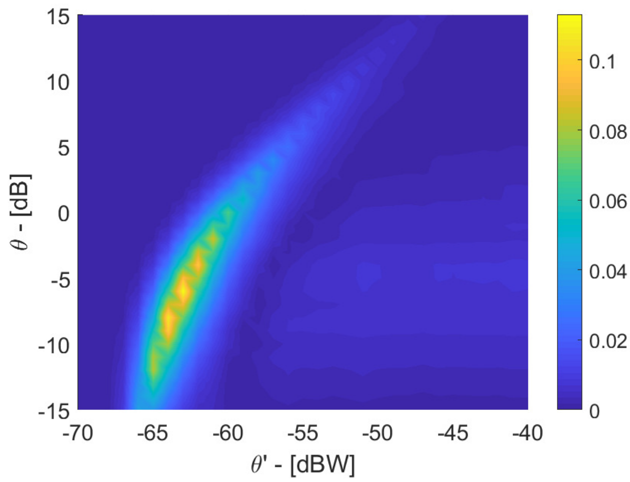

(c) Error

Figure 4.3: JPCE - HomNet : $\lambda = 10^{-6}[BS/m^2]$, $P = 30[dBm]$, $\alpha = 2.5$.

4.4.2 Heterogeneous Network

Figures 4.4 and 4.5 compare the CP obtained by equation (4.37) and the EP obtained by equation (4.31) with numerical results. Figure 4.6 shows the JPCE obtained by MC simulations (a), by SG (b) and the absolute observed error (c). For a HetNet, the same observations on the accuracy of the CP, EP and JPCE can be made based on these Figures. Therefore, the model derived in this chapter for the JPCE of a HetNet is considered accurate down to sufficiently high exposure thresholds.

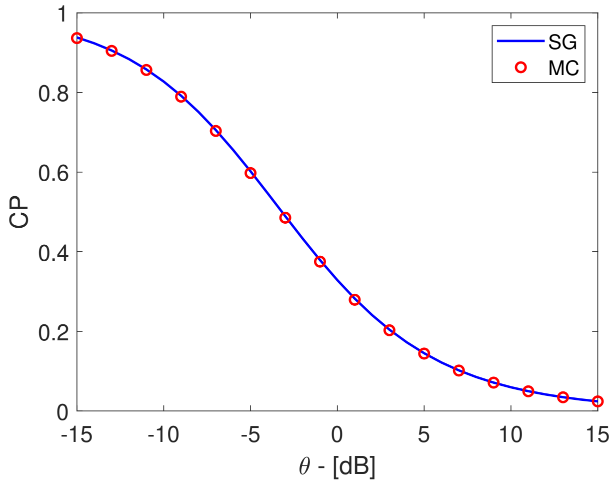

Figure 4.4: CP - HetNet : $(\lambda_1, \lambda_2) = (10^{-7}, 10^{-5})[BS/m^2]$, $(P_1, P_2) = (60, 30)[dBm]$, $(\alpha_1, \alpha_2) = (2.5, 2.7)$.

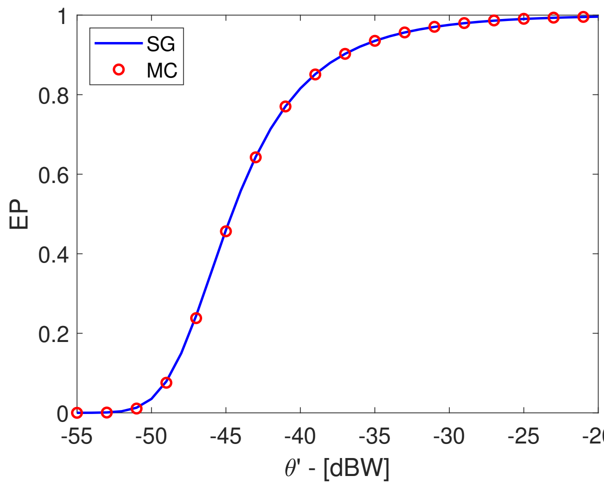

Figure 4.5: EP- HetNet : $(\lambda_1, \lambda_2) = (10^{-7}, 10^{-5})[BS/m^2]$, $(P_1, P_2) = (60, 30)[dBm]$, $(\alpha_1, \alpha_2) = (2.5, 2.7)$.

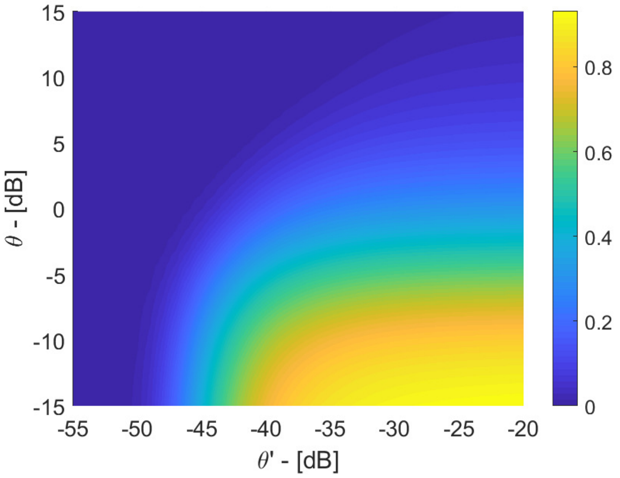

(a) Monte-Carlo Simulations

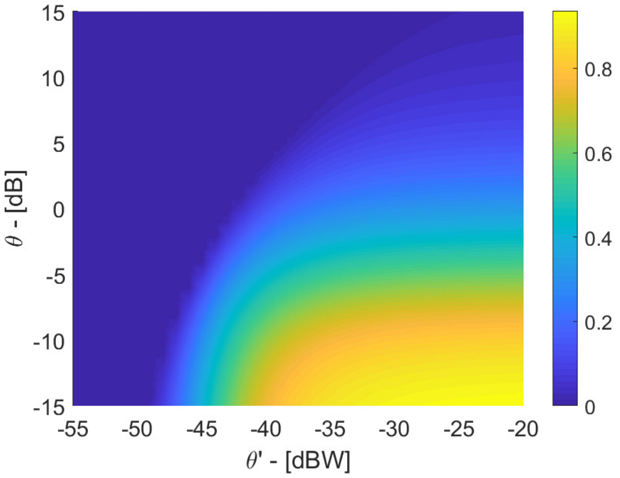

(b) Stochastic Geometry

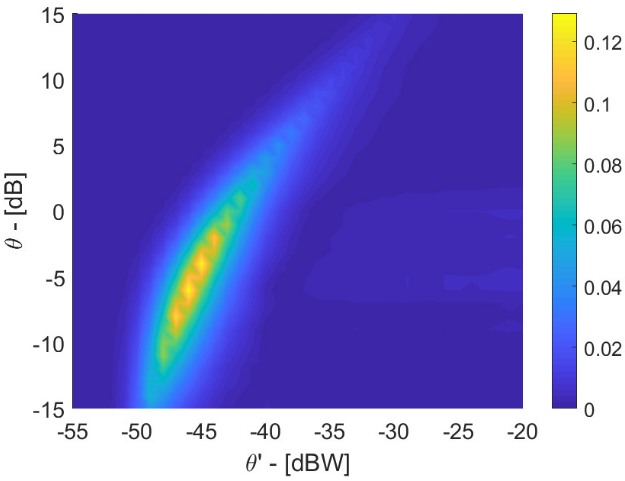

(c) Error

Figure 4.6: JPCE - HetNet : $(\lambda_1, \lambda_2) = (10^{-7}, 10^{-5})[BS/m^2]$, $(P_1, P_2) = (60, 30)[dBm]$, $(\alpha_1, \alpha_2) = (2.5, 2.7)$.

Chapter 5

Optimization Problem 1: Joint Optimization of Coverage and Exposure - Heterogeneous Network Deployment with Common Path-Loss

In this chapter, a network deployment optimization problem on the tier densities and transmission powers is formulated and solved. The purpose is to jointly optimize both coverage and exposure in a HetNet. In order to propose realistic solutions to this existing problem, a constrained optimization is introduced with the performance metric $\mathbb{F}(\theta, \theta')$ as an objective function. In this study, the HetNet is modelled assuming a **common Path-Loss** and **Rayleigh fading**.

The double numerical integration inherent to the Gil-Pelaez based model does not allow to obtain an analytical solution to the optimization. Therefore, the first part of this chapter is dedicated to the formulation of a tractable model for the JPCE.

Based on this tractable model, two linear optimization problems are introduced: one on the tier densities and a second on both tier densities and transmission powers. The analysis focuses on a 2TN and optimal solutions are derived in closed-form. Nevertheless, this restricted analysis allows the conclusion to be extended to a more general K-tiers case. The main outcome of this optimization shows that the maximization of both coverage and exposure is obtained by minimizing the tier densities and transmission powers. Furthermore, the performances are similar in a HomNet or a HetNet once they are optimized. These conclusions only apply to

HetNets with a common path-loss.

5.1 Performance Metrics: Tractable Models

The framework used to develop a closed-form expression of the JPCE is based on a different approach than the one based on the Gil-Pelaez theorem. This approach is explained in [19] to express the CP with a tractable model. However, this model relies on assumptions which limit its validity. In this section, an additional assumption, the **high SIR assumption**, is made on EXPO in order to further reduce the complexity. By comparing the theoretical and simulated results, the new model is considered an accurate approximation of the JPCE down to $2[dB]$ SIR thresholds and sufficiently high exposure thresholds.

As a reminder, a HeNet is modelled by K independent HPPPs denoted by $\mathbf{\Phi}_k$, and characterized by their density λ_k and transmission power P_k. A common PLE α is assumed for all the tiers and the amplitude of the channel gain follows a Rayleigh distribution.

5.1.1 High SIR Assumption

Assuming the network performances are evaluated at high SIR (SIR $\gg 1$), one can state that the useful signal dominates the interference in the exposure term. Consequently, the interfering signal can be neglected in EXPO.

Definition 5.1 (High SIR Assumption)

$$\begin{aligned} \mathrm{SIR} &\gg 1 \\ \mathrm{EXPO} &\simeq \mathcal{S} \end{aligned} \tag{5.1}$$

The EP and the JPCE are then defined as follows:

$$\mathbb{P}_{\mathrm{expo}}(\theta') = \mathbb{P}\left[\mathcal{S} < \theta'\right] \tag{5.2}$$

$$\mathbb{F}(\theta, \theta') = \mathbb{P}\left[\frac{\mathcal{S}}{\mathcal{I}} > \theta, \mathcal{S} < \theta'\right] \tag{5.3}$$

This strong assumption leads to an approximation, a lower bound of EXPO and limits the analysis to high SIR coverage. The validity of this assumption is evaluated in section 5.1.5.

5.1.2 Power Association Rule Assumption

In the previous chapter, the performance metric $\mathbb{F}(\theta, \theta')$ is derived according to a DAR. With a **Power Association Rule** (PAR), the typical user chooses to associate with the strongest BS in terms of instantaneously received power. As the fading is not averaged out in the association process, each BS becomes a potential candidate to serve the user.

Definition 5.2 (Power Association Rule)

For a KTN, the useful signal is defined as follows:

$$\mathcal{S} = \max_{r_{i,k} \in \mathbf{\Phi_k},\, k \in 1,\ldots,K} P_k |h|^2 r_{i,k}^{-\alpha} \tag{5.4}$$

The interfering signal is then defined as follows:

$$\mathcal{I} = \sum_{k=1}^{K} \sum_{r_{i,k} \in \mathbf{\Phi_k}} P_k |h|^2 r_{i,k}^{-\alpha} - \mathcal{S} \tag{5.5}$$

Unlike the the DAR, no interference boundaries can be defined for a PAR. This major difference changes the way the performance metric is developed. In section 5.1.5, a comparison between both association rules is provided.

5.1.3 Coverage Probability

A tractable model of the CP based on a PAR is derived in [19]. As mentioned in the previous section, the PAR implies that each BS is a potential candidate. For that reason, the performance metric can not be derived for a fixed serving distance and fixed interference boundaries, and afterwards be averaged over the distance.

The CP is now defined as the probability of the union of BSs providing a SIR higher than a threshold θ.

Proposition 5.1 (Coverage Probability)

For $\theta > 1$, in a KTN with a common PLE and assuming a PAR, the CP is defined as follows [19]:

$$\begin{aligned}\mathbb{P}_{\mathrm{cv}} &= \mathbb{P}\left[\bigcup_{r_{i,k}\in\mathbf{\Phi_k},\, k\in 1,\dots,K} \mathrm{SIR}(r_{i,k}) > \theta\right] \\ &= \frac{\theta^{-2/\alpha}\alpha\sin\left(\frac{2\pi}{\alpha}\right)}{2\pi}\end{aligned} \tag{5.6}$$

Proof : see Appendix A.2

Proposition 5.1 relies on Lemma 2.1 defined in chapter 2. This Lemma characterizes the number of potential BSs that the typical user can connect to [19]. $\{a_1, a_2, ..., a_n\}$ correspond to the received powers from each BS and c_i to the SIR of the i^{th} BS [19]. From this Lemma and assuming $\theta > 1$, the typical user can connect to at most one BS at any time. Therefore, the CP can be defined as the sum of the probabilities that each BS provides a SIR higher than θ because all these events are mutually exclusive.

From Proposition 5.1, one can observe that the CP is also independent of the tier densities and transmission powers for a PAR.

As mentioned in the proof of Proposition 5.1, the PAR asks us to consider the interference as the sum of the received powers from all the BSs. Hence, the interference defined in this framework is an upper bound because it includes the useful signal. Despite this approximation, expression 5.6 is an accurate estimation of the CP down to $-4[dB]$ (validation shown in [19]).

5.1.4 Joint Probability of Coverage and Exposure

Under the assumption of high SIR and PAR, the JPCE is defined as the probability of the union of BSs providing a SIR higher than θ and an useful signal power lower than θ'.

Proposition 5.2 (Joint Probability of Coverage and Exposure)

For $\theta > 1$, in a KTN with a common PLE, and under the assumption of high SIR and PAR, the JPCE is defined as follows:

$$\begin{aligned}\mathbb{F}(\theta,\theta') &= \mathbb{P}\left[\bigcup_{r_{i,k}\in\mathbf{\Phi_k},\, k\in 1,\ldots,K} (\mathrm{SIR}(r_{i,k}) > \theta, \mathrm{EXPO}(r_{i,k}) < \theta')\right] \\ &= \frac{\theta^{-2/\alpha}\alpha\sin\left(\frac{2\pi}{\alpha}\right)}{2\pi} - \frac{\sum_{k=1}^{K} 2\pi\lambda_k P_k^{2/\alpha}\Gamma(\frac{2}{\alpha})}{\alpha\theta'^{2/\alpha}}\end{aligned} \tag{5.7}$$

Proof : see Appendix A.2

The approach to derive this performance metric is similar to that introduced in [19]. From Lemma 2.1 and assuming $\theta > 1$, at most one BS can provides a SIR higher than θ and an EXPO lower than θ' at any time. Therefore, the joint probability can also be defined as the sum of the probabilities of each BS.

Final expression (5.7) is composed of two terms, the CP and a second related to the EP.

It is worth to emphasize the tractability of the Gil-Pelaez based model and the one derived in this chapter. It highlights the reason why the high SIR and PAR assumptions are made. The validity and accuracy of Proposition 5.2 are evaluated in the following section.

5.1.5 Numerical Results - Validations

In this section, the validity of both assumptions are first verified with MC simulations by considering a HomNet with a unit transmission power. The accuracy of Proposition 5.2 is evaluated by comparing the theoretical model and simulated results for a 2TN.

Validity of the High SIR Assumption

To evaluate the validity, the error between expressions (3.28) and (5.3) is computed and analysed for different HPPP densities λ. The MC simulations are generated with a PAR.

$$Error = \mathbb{P}\left[\frac{\mathcal{S}}{\mathcal{I}} > \theta, \mathcal{S} < \theta'\right] - \mathbb{P}\left[\frac{\mathcal{S}}{\mathcal{I}} > \theta, \mathcal{S}+\mathcal{I} < \theta'\right]$$

Figure 5.1 shows the performance metric $\mathbb{F}(\theta, \theta')$ for $\lambda = 5 * 10^{-6}[BS/m^2]$ and Figures 5.2, the observed error for three BS densities. Under the high SIR assumption, expression (5.3) is an upper bound of the real metric definition (3.28). Indeed, the observed error assumes positive values. No matter the BS density, the error is smaller than 0.02 for SIR thresholds $\theta > 4[dB]$ and about a thousandth for $\theta > 6[dB]$. The main error is observed at low SIR ($\theta < 4[dB]$) in a $10[dB]$ wide region. Changing the BS density simply moves the position of this region with respect to θ'. Finally, these simulations prove the validity of the high SIR assumption, especially for SIR thresholds higher than $6[dB]$.

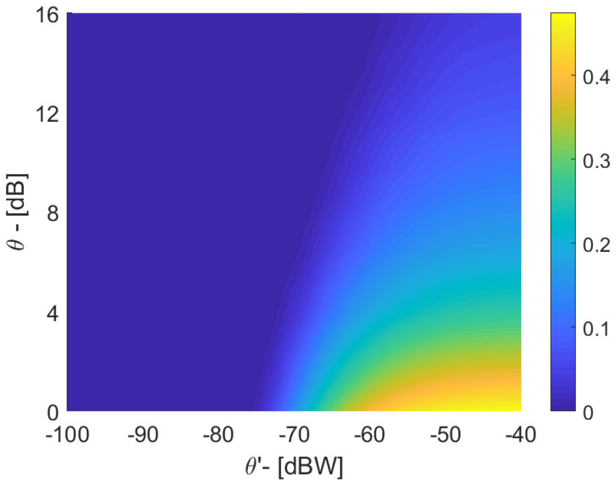

Figure 5.1: $\mathbb{F}(\theta, \theta')$ under no high SIR assumption: $\lambda = 50^{-6}[BS/m^2]$, $P = 30[dBm]$, $\alpha = 3.2$.

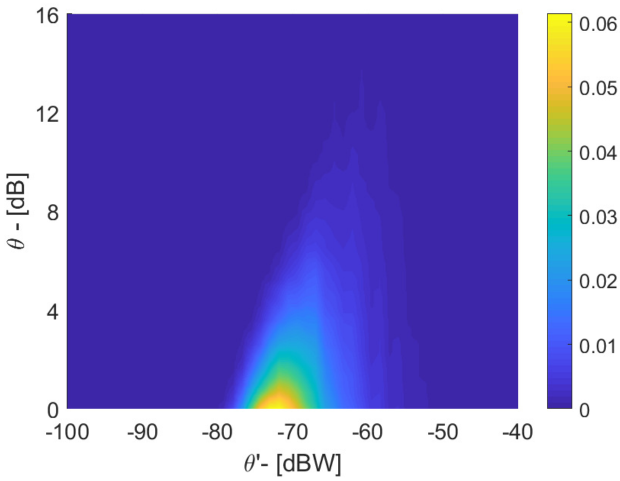

(a) $\lambda = 5 * 10^{-6}[BS/m^2]$

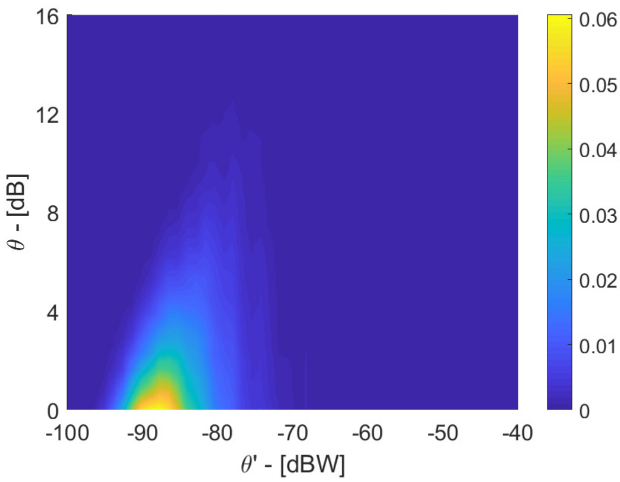

(b) $\lambda = 5 * 10^{-7}[BS/m^2]$

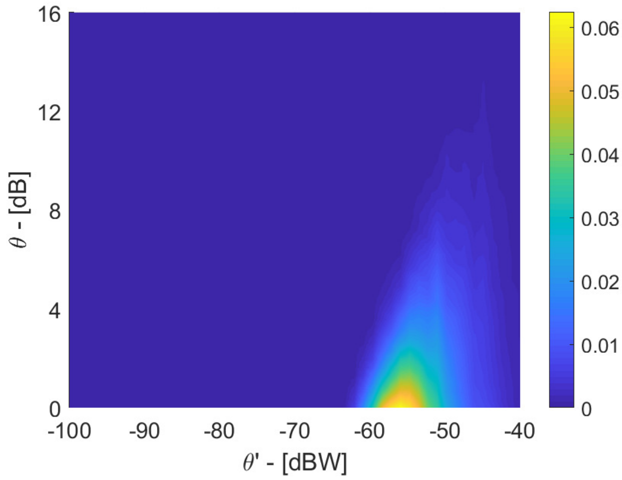

(c) $\lambda = 5 * 10^{-5}[BS/m^2]$

Figure 5.2: High SIR Assumption - Error: $P = 30[dBm]$, $\alpha = 3.2$.

Validity of the Power Association Rule

This assumption is verified by comparing the CP for a DAR and PAR in Figure 5.3. As equation (5.6) and studies in SG show, the CP does not depend on the BS density in a HomNet. Hence, the results are only generated for a given density λ.

For SIR thresholds $\theta > 5[dB]$, the DAR and PAR provide similar performances. It means that at high SIR, the serving BSs in terms of LTARP and instantaneously received power are the same.

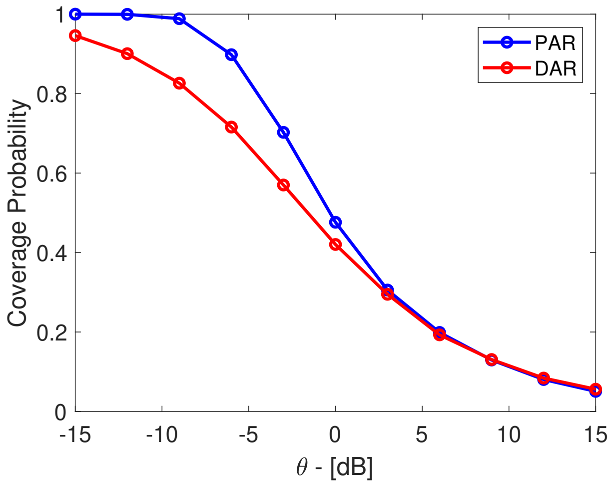

Figure 5.3: CP - DAR and PAR: $\lambda = 5 * 10^{-7}[BS/m^2]$, $P = 30[dBm]$, $\alpha = 3.2$.

Accuracy of Proposition 5.2

The accuracy of Proposition 5.2 is evaluated for a 2TN. The MC simulations are generated for both association rules. A comparison between the SG model and numerical results is then proposed for both rules. Figures 5.4 show the performance metric $\mathbb{F}(\theta, \theta')$ obtained by numerical and theoretical results, and the observed error assuming a PAR. Figures 5.5 show the same results assuming a DAR. For similar reasons mentioned in section 4.4, the analytical expression is truncated to positive values.

Due to this truncation, an edge effect is observable in Figures 5.4(c) and 5.5(b). No matter the association rule, expression (5.7) is accurate to the thousandth for SIR thresholds higher than $2[dB]$ ($0[dB]$ for the PAR). At low SIR ($\theta < 2[dB]$), the error is much higher compared to a DAR, a result consistent with the validation of the PAR.

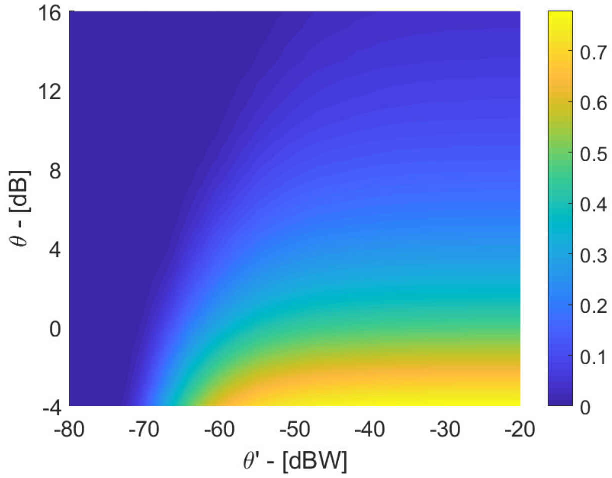

(a) Monte-Carlo

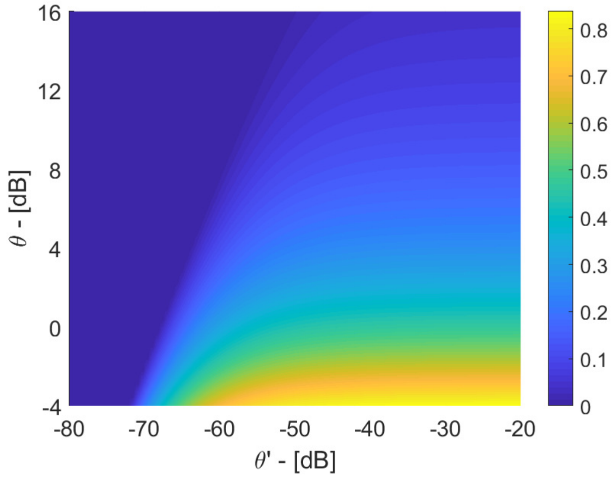

(b) Stochastic Geometry

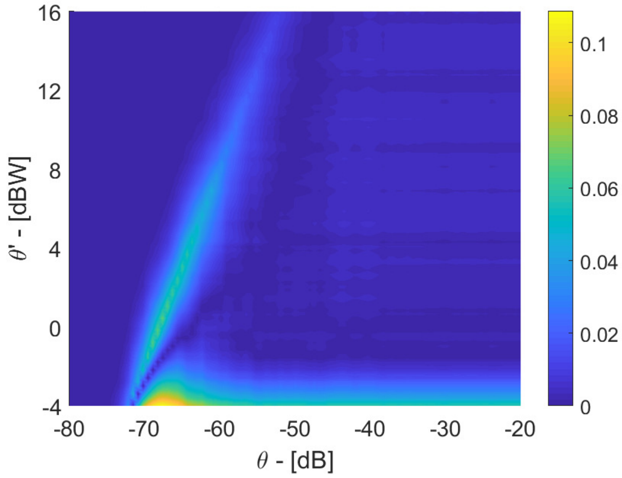

(c) Error

Figure 5.4: $\mathbb{F}(\theta, \theta')$ - PAR: $(\lambda_1, \lambda_2) = (5 * 10^{-7}, 5 * 10^{-6})[BS/m^2]$, $(P_1, P_2) = (45, 30)[dBm]$, $\alpha = 3.2$

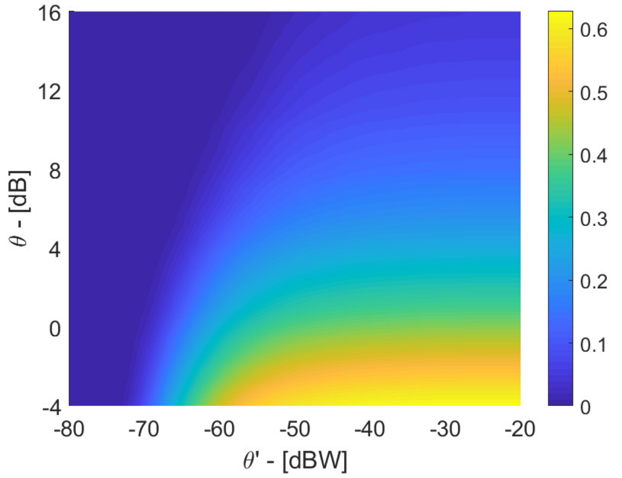

(a) Monte-Carlo

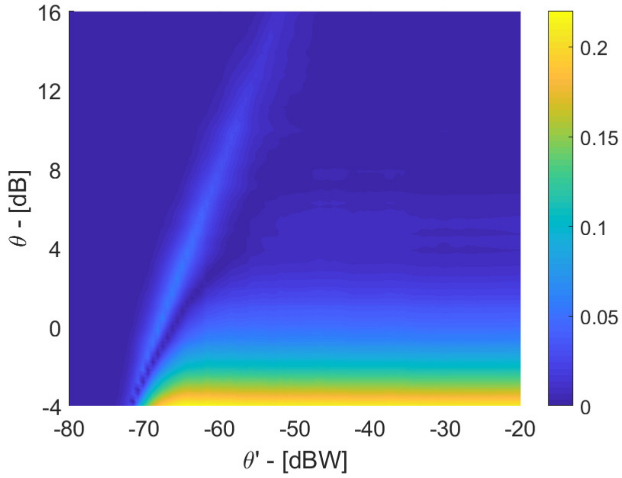

(b) Error

Figure 5.5: $\mathbb{F}(\theta, \theta')$ - DAR: $(\lambda_1, \lambda_2) = (5 * 10^{-7}, 5 * 10^{-5})[BS/m^2]$, $(P_1, P_2) = (45, 30)[dBm]$, $\alpha = 3.2$

5.2 Constraints

The constraints formulated in this work are inspired by optimization problems introduced in [7]. In this paper, the authors define a constraint on the minimum received power, some constraints on the fraction loads and deployment costs (specifically related to their study). In this chapter, the joint optimization problems base on these two first constraints.

5.2.1 Minimum Received Power

A HetNet is designed to ensure a **Minimum Received Power** (MRP) from the serving BSs. This constraint is defined as the probability that the useful signal power is lower than a given threshold δ and is applied with a maximum probability ϵ.

Proposition 5.3 (Constraint c_1: MRP)

The constraint on the MRP in a KTN is defined as follows:

$$\mathbb{P}\left[\mathcal{S} < \delta\right] < \epsilon, \quad 0 < \epsilon < 1$$

$$\text{expressed as:} \quad \sum_{k=1}^{K} \lambda_k P_k^{2/\alpha} > \epsilon' \tag{5.8}$$

$$\text{where} \quad \epsilon' = \frac{\alpha \delta^{2/\alpha} \log \frac{1}{\epsilon}}{2\pi \Gamma(\frac{2}{\alpha})} \tag{5.9}$$

Proof : See Appendix A.2

5.2.2 Minimum Fraction Loads

In HetNet optimization, a **Minimum Fraction Load** (MFL) constraint is applied on each tier to ensure a minimum level of utilization by the UEs. This is necessary to avoid a trivial solution with only one tier. The tier fraction load is defined as the probability that a user is served by a given tier. This quantity is derived in chapter 4 with a DAR. As mentioned in section 5.1.5, at high SIR, the PAR and DAR provide similar performances. Therefore, unlike the objective function and constraint c_1, the expressions of these constraints on the MFLs are derived with a DAR. For a common PLE, the expressions are in closed-from.

Proposition 5.4 (Constraints $c_{2,k}$: MFLs)

The constraints on the MFLs in a KTN are defined as follows:

$$\mathcal{A}_k > \eta_k \quad \forall\, k \in 1, ..., K \quad \text{such that} \quad \sum_{k=1}^{K} \eta_k \leq 1$$

$$\text{where} \quad \mathcal{A}_k = \frac{\lambda_k P_k^{2/\alpha}}{\sum_{i=1}^{K} \lambda_i P_i^{2/\alpha}} \tag{5.10}$$

Proof : See Appendix A.2 (Proof of Proposition 4.6)

5.3 Optimization Problem 1: Tier Densities

In this section, the densities of a KTN are optimized to maximize the JPCE. This network deployment optimization problem is linear. Therefore, from optimization theory, the problem is convex and the optimal solution is located on the constraints. For a 2TN, an analytical solution is derived by combining analytical and graphical methods.

5.3.1 K-tiers Network: Optimization Problem Formulation

Let $\{\lambda_k\}_{k=1}^{K}$ denote the set of the tier densities. The objective function of optimization problem 1 (**P1**) is defined as follows:

$$\begin{aligned}\mathcal{F}(\{\lambda_k\}_{k=1}^{K};\theta,\theta') &= \mathbb{F}(\theta,\theta') \\ &= \frac{\theta^{-2/\alpha}\alpha\sin\left(\frac{2\pi}{\alpha}\right)}{2\pi} - \frac{\sum_{k=1}^{K}2\pi\lambda_k P_k^{2/\alpha}\Gamma(\frac{2}{\alpha})}{\alpha\theta'^{2/\alpha}}\end{aligned} \tag{5.11}$$

Let us formulate **P1**. The tier densities are optimized in order the maximize the JPCE under constraints on the MRP and MFLs.

$$\begin{aligned}&\max_{\{\lambda_k\}_{k=1}^{K}} \mathcal{F}(\{\lambda_k\}_{k=1}^{K};\theta,\theta') \\ \text{such that}\quad & c_1: \quad \sum_{k=1}^{K}\lambda_k P_k^{2/\alpha} > \epsilon' \\ & c_{2,k}: \quad \mathcal{A}_k > \eta_k, \quad \sum_{k=1}^{K}\eta_k \le 1 \quad \forall\, k \in 1,...,K \\ & c_{3,k}: \quad \lambda_k \ge 0\end{aligned}$$

5.3.2 2-tiers Network: Analytical Solution

For a 2TN, **P1** is reduced to this formulation.

Definition 5.3 (P1 - 2-tiers Network)

$$\max_{\lambda_1,\lambda_2} \quad \frac{\theta^{-2/\alpha}\alpha \sin\left(\frac{2\pi}{\alpha}\right)}{2\pi} - 2\pi\left[\frac{\lambda_1 P_1^{2/\alpha}\Gamma(\frac{2}{\alpha})}{\alpha\theta'^{2/\alpha}} + \frac{\lambda_2 P_2^{2/\alpha}\Gamma(\frac{2}{\alpha})}{\alpha\theta'^{2/\alpha}}\right]$$

$$\begin{aligned}
\text{such that} \quad & c_1: & & \lambda_1 P_1^{2/\alpha} + \lambda_2 P_2^{2/\alpha} > \epsilon' \\
& c_{2,1}: & & (1-\eta_1)\lambda_1 P_1^{2/\alpha} - \eta_1\lambda_2 P_2^{2/\alpha} > 0 \\
& c_{2,2}: & & -\eta_2\lambda_1 P_1^{2/\alpha} + (1-\eta_2)\lambda_2 P_2^{2/\alpha} > 0, \quad \eta_1 + \eta_2 \leq 1 \\
& c_{3,1}: & & \lambda_1 \geq 0 \\
& c_{3,2}: & & \lambda_2 \geq 0
\end{aligned}$$

Let $\mathcal{R}$ denote the feasible region of **P1**:

$$\mathcal{R} = \Big\{(\lambda_1,\lambda_2) \in \mathbb{R}_+^2 | \lambda_1 P_1^{2/\alpha} + \lambda_2 P_2^{2/\alpha} > \epsilon', (1-\eta_1)\lambda_1 P_1^{2/\alpha} - \eta_1\lambda_2 P_2^{2/\alpha} > 0,$$
$$-\eta_2\lambda_1 P_1^{2/\alpha} + (1-\eta_2)\lambda_2 P_2^{2/\alpha} > 0\Big\} \tag{5.12}$$

Figure 5.6 shows a visualization of the constraints and feasible domain (*grey*).

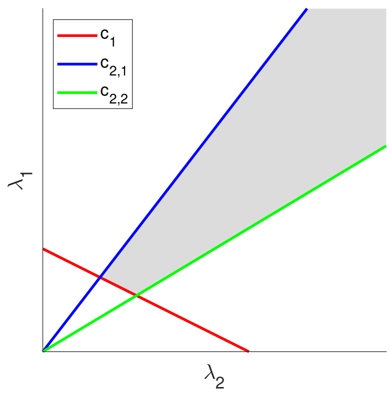

Figure 5.6: **P1** - Feasible Region

To propose an optimal solution, let us first derive the gradient of the objective function.

$$\nabla\mathcal{F}(\lambda_1,\lambda_2) = \begin{bmatrix} \dfrac{\partial\mathcal{F}}{\partial\lambda_1}(\lambda_1,\lambda_2) \\ \dfrac{\partial\mathcal{F}}{\partial\lambda_2}(\lambda_1,\lambda_2) \end{bmatrix} = \frac{2\pi\Gamma\left(\frac{2}{\alpha}\right)}{\alpha\theta'^{2/\alpha}} \begin{bmatrix} -P_1^{2/\alpha} \\ -P_2^{2/\alpha} \end{bmatrix} \tag{5.13}$$

From equation (5.13), one can therefore formulate the optimal solution as follows:

$$(\lambda_1^*,\lambda_2^*) = \underset{(\lambda_1,\lambda_2)\in\mathcal{R}}{\arg\min}\ \lambda_1 P_1^{2/\alpha} + \lambda_2 P_2^{2/\alpha} \tag{5.14}$$

One can deduce that the set of optimal solutions is located on the constraint c_1. From the graphical visualization (Fig. 5.6), this set is delimited by the intersections $(c_1, c_{2,1})$ and $(c_1, c_{2,2})$. Consequently, the analytical solution to **P1** can be formulated as follows:

Proposition 5.5 (P1 - Analytical Solution $(\lambda_1^*,\lambda_2^*)$**)**

The set of optimal solutions $(\lambda_1^*,\lambda_2^*)$ to **P1** for a 2TN is defined as follows:

$$\lambda_1^* = \frac{\epsilon' - \lambda_2^* P_2^{2/\alpha}}{P_1^{2/\alpha}}, \quad \text{with} \quad \lambda_2^* \in \left[\frac{\epsilon'\eta_2}{P_2^{2/\alpha}}, \frac{\epsilon'(1-\eta_1)}{P_2^{2/\alpha}}\right] \tag{5.15}$$

Proof : see Appendix A.2

5.4 Optimization Problem 1': Tier Densities and Transmission Powers

A more general problem formulation can be extended to a joint optimization on the tier densities and transmission powers. In this section, a new optimization problem is introduced and an analytical solution is derived for a 2TN.

5.4.1 K-tiers Network: Optimization Problem Formulation

By analysing the expressions of the objective function and constraints, one can observe that the tier densities λ_k and transmission powers P_k are expressed under the same form $\lambda_k P_k^{2/\alpha}$. Hence, let us define a new variable x_k:

$$x_k = \lambda_k P_k^{2/\alpha} \tag{5.16}$$

Optimization problem 1' (**P1'**) can be formulated with respect to $\{x_k\}_{k=1}^K$.

$$\max_{\{x_k\}_{k=1}^K} \frac{\theta^{-2/\alpha}\alpha \sin\left(\frac{2\pi}{\alpha}\right)}{2\pi} - \frac{\sum_{k=1}^K 2\pi x_k \Gamma(\frac{2}{\alpha})}{\alpha\theta'^{2/\alpha}}$$

$$\begin{aligned}\text{such that} \quad & c_1 : && \sum_{k=1}^K x_k > \epsilon' \\ & c_{2,k} : && \frac{x_k}{\sum_{i=1}^K x_i} > \eta_k, \quad \sum_{k=1}^K \eta_k \leq 1 \quad \forall\, k \in 1, ..., K \\ & c_{3,k} : && x_k \geq 0\end{aligned}$$

5.4.2 2-tiers Network - Analytical Solution

A similar analytical and graphical proof can be applied to propose an analytical solution to **P1'** for a 2TN.

Proposition 5.6 (P1' - Analytical Solution (x_1^*, x_2^*)**)**

The set of optimal solutions (x_1^*, x_2^*) to **P1'** for a 2TN is defined as follows:

$$x_1^* = \epsilon' - x_2^*, \quad \text{with} \quad x_2^* \in [\epsilon'\eta_2, \epsilon'(1-\eta_1)] \tag{5.17}$$

By substituting (5.16) into (5.17), **P1** and **P1'** lead to the same optimal solution. By inserting any point (x_1^*, x_2^*) or $(\lambda_1^*, \lambda_2^*)$ into the objective function, the JPCE can be evaluated at the optimal solution.

Proposition 5.7 (P1, P1' - Optimal JPCE)

The objective function of **P1** or **P1'** evaluated at the any optimal solution for a 2TN is given by:

$$\mathcal{F}(\lambda_1^*, \lambda_2^*; \theta, \theta') = \mathcal{F}(x_1^*, x_2^*; \theta, \theta') = \frac{\theta^{-2/\alpha}\alpha \sin\left(\frac{2\pi}{\alpha}\right)}{2\pi} - \frac{\delta^{2/\alpha}\log\left(\frac{1}{\epsilon}\right)}{\theta'^{2/\alpha}} \tag{5.18}$$

5.5 Numerical Results and Discussions

In this last section, numerical results are first provided to validate the theoretical analysis of **P1** and **P1'** for a 2TN. Afterwards, some specific conclusions to HetNets with a common path-loss are drawn on the basis of this optimization.

Figures 5.7 and 5.8 show a global visualization of **P1** and **P1'**, the objective functions (*colormap*), constraints and optimal solutions, that validate the theoretical analysis. Indeed, both optimal JCPEs are equal to 0.104. Table 5.1 gives the optimal solution at the intersection $(c_1, c_{2,1})$. By substituting λ_k^* and P_k into x_k, the same numerical values as x_k^* are obtained.

	$\lambda^*[BS/m^2]$	$P[W]$	$x = \lambda^* P^{2/\alpha}$
Tier 1	$2.83 * 10^{-5}$	31.62	$2.45 * 10^{-4}$
Tier 2	$3.67 * 10^{-4}$	1	$3.67 * 10^{-4}$

Table 5.1: **P1** and **P1'** - Optimal Solutions: $\theta = 10[dB]$, $\theta' = -10[dBW]$, $\epsilon = 0.1$, $\delta = -20[dBm]$, $(\eta_1, \eta_2) = (0.4, 0.4)$, $\alpha = 3.2$.

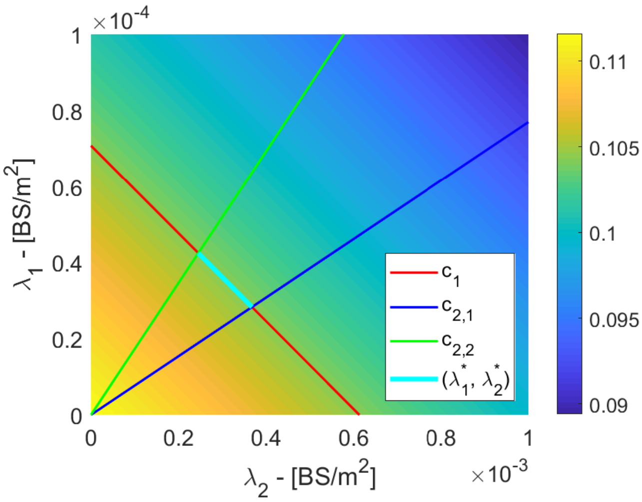

Figure 5.7: **P1**: $\theta = 10[dB]$, $\theta' = -10[dBW]$, $\epsilon = 0.1$, $\delta = -20[dBm]$, $(\eta_1, \eta_2) = (0.4, 0.4)$, $(P_1, P_2) = (45, 30)[dBm]$, $\alpha = 3.2$.

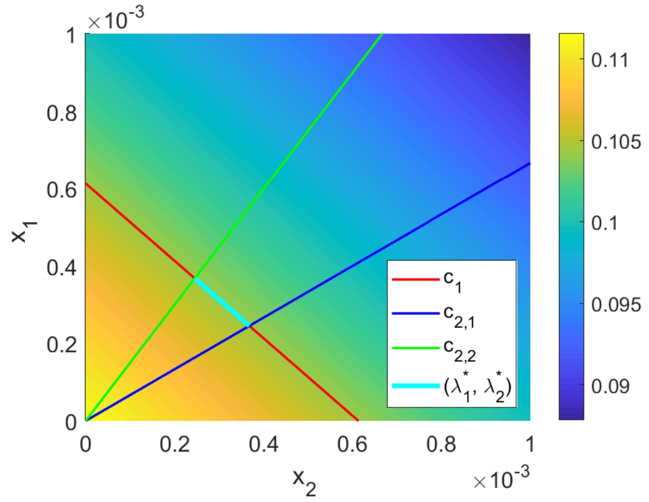

Figure 5.8: **P1'**: $\theta = 10[dB]$, $\theta' = -10[dBW]$, $\epsilon = 0.1$, $\delta = -20[dBm]$, $(\eta_1, \eta_2) = (0.4, 0.4)$, $\alpha = 3.2$.

Figure 5.9 shows expression (5.18) with respect to δ and for different PLEs α. The observation is straightforward. No matter the value of δ, the JPCE increases in propagation environments with higher losses. By applying a higher constraint on the MRP, the EP logically decreases and so does the JPCE.

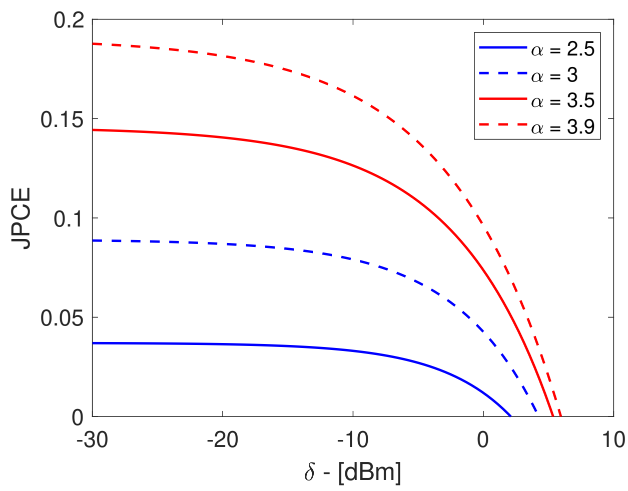

Figure 5.9: Optimal JPCE - Impact of δ and α: $\theta = 10[dB]$, $\theta' = -10[dBW]$, $\epsilon = 0.1$.

The formulation and resolution of **P1'** show that a joint optimization on the tier densities and transmission powers does not improve the performance in terms of

JPCE. An optimization on the densities or the powers provides the same result. Both quantities depend on each other as shows the variable x_k.

For a 2TN, the gradient of the objective function is orthogonal to the MRP constraint. It shows that a maximization of the performance metric goes through a minimization of the tier densities (or x_k). This observation on the gradient also applies to a KTN. In that general case, the set of optimal solutions is also located on the MRP constraint and delimited by the constraints on the MFLs.

Proposition 5.7 gives an expression of the JPCE evaluated at any optimal solution. This expression is derived in section 5.4.2 for a 2TN. Optimizing a KTN will also leads to equation (5.18). An intuitive reasoning is sufficient to justify this conclusion. The gradient of the objective function shows that the set of optimal solutions is located on the constraint c_1. By substituting the line equation of c_1 into equation (5.11), expression (5.18) is obtained. From Proposition 5.7, one can deduce that the optimal JPCE does not depend on the tier characteristics. For given thresholds θ, θ', it only depends on the MRP constraint parameters δ and ϵ. As a result, a HomNet provides the same performances.

Chapter 6

Optimization Problem 2: Joint Optimization of Coverage and Exposure - Heterogeneous Network Expansion

In chapter 5, a complete HetNet deployment optimization problem is introduced. However, in most practical scenarios, at least some of tiers are already deployed (e.g., macro BS) [7]. In this chapter, a optimization problem on the tier densities and transmission powers is formulated for a tier addition in the network. The expansion of a HetNet allows to easier study the impact of different conditions of wave propagation in each tier, which is the main purpose of this second problem. The optimization studied in this chapter leads to non-realistic solutions. However, the developments of these solutions allows to understand some specific behaviors of HetNets. The main outcome of this chapter highlights the interest of deploying HetNets when the tiers experience different conditions of wave propagation.

This second optimization problem aims to maximize the JPCE in the added tier while ensuring sufficient coverage in the other tiers. Hence, all the performance metrics and constraints are now defined per tier in this chapter. Optimization problem 2 focuses on a 2TN. For this specific case, a closed-form analytical solution is derived by graphical interpretations. The study introduced in this chapter can be liken to a practical scenario in which a first tier composed of macro BSs ensures the coverage in rural area and a second composed of micro BSs will be deployed in urban area. The propagation conditions of these two tiers are modelled by different path-loss.

When considering different path-loss in a HetNet, studies in SG usually associated specific PLEs to each tier (e.g. [1], [20]). However, this modelling has some disadvantages. The first section of this chapter is dedicated to the introduction of a new model for different path-loss in HetNets. This model, even not perfect, is preferred to the one commonly used in SG because it leads to closed-form expressions. As in chapter 5, all the expressions are developed assuming **Rayleigh fading**.

6.1 Different Path-Loss Model

In order to differentiate the propagation conditions in a HetNet, specific PLEs are usually associated to each tier. This mathematical model, referenced as **model 1**, is simple but not always the most realistic or coherent. To highlight this, let us consider two cases corresponding to the optimization problem introduced in this chapter. A first tier is deployed in rural areas with a PLE α_1 and a second in urban areas with α_2. In order to model the higher losses in urban environments, it is assumed that $\alpha_2 > \alpha_1$. **Model 1** follows the definition of the useful signal and interfering signal given in Definition 4.2.

In Figure 6.1, the user is located in urban area and therefore, is served by the second tier. The usual model states that the interfering signal experiences a path-loss associated to a propagation in rural environment (α_1). This provides an upper bound of the interference and consequently, an lower bound of the SIR. In Figure 6.2, it is the opposite configuration. The usual model leads to a lower bound of the interfering signal and an upper bound of the SIR.

These two examples show that **model 1** does not take into account the environment where the user is located. The new model defined in the next section proposes a different approach for the choice of the PLE associated to the interfering signal.

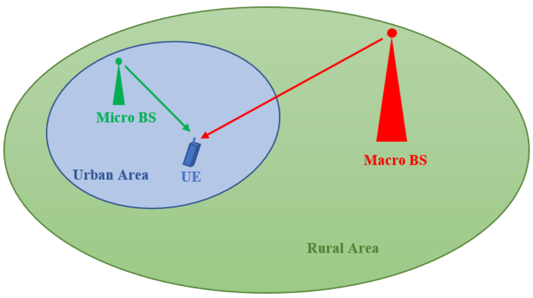

Figure 6.1: Different Path-Loss: Case 1

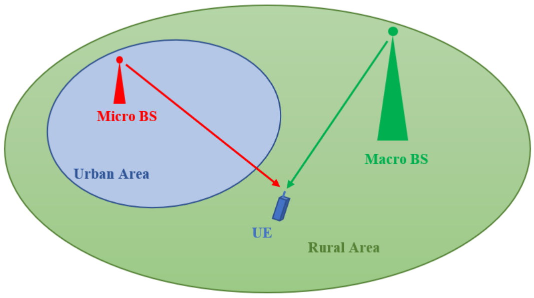

Figure 6.2: Different Path-Loss: Case 2

6.1.1 New Different Path-Loss Model

The new model, referenced as **model 2**, defines the PLE of the interfering signal based on the environment where the user is located. One can say that if the user is in rural area, then he is served by a BS deployed in rural area, as shown in Figures 6.2. Hence, **model 2** assumes that the PLE of the interfering signal is equal to the one of the serving tier. With a PAR, this model is formulated as follows:

Definition 6.1 (Different Path-Loss Model 2)

Assuming a PAR and the typical user is served by the k^{th}-tier in a KTN, the useful signal is defined as follows:

$$\mathcal{S} = \max_{r_{i,k} \in \mathbf{\Phi_k},\, k \in 1,\ldots,K} P_k |h|^2 r_{i,k}^{-\alpha_k} \tag{6.1}$$

The interfering signal is then defined as follows:

$$\mathcal{I} = \sum_{k=1}^{K} \sum_{r_{i,k} \in \mathbf{\Phi_k}} P_k |h|^2 r_{i,k}^{-\alpha_k} - \mathcal{S} \tag{6.2}$$

Definition 6.1 is formulated for a PAR because all the expressions used in this chapter are derived based on this rule.

6.1.2 Comparison with a Hybrid Model

In this section, a comparison between **model 1** and **model 2** is provided. This comparison bases on a hybrid model which is defined with a dual-slope path loss function. The interest of using a dual-slope is to model the two propagation mediums with two different PLEs. From equation (3.4), let us remind this function:

$$PL_{\text{dual}}(r; \alpha_0, \alpha_1) = \begin{cases} r^{-\alpha_0}, & r \leq d_{th} \\ d_{th}^{\alpha_1 - \alpha_0} r^{-\alpha_1}, & r > d_{th} \end{cases} \tag{6.3}$$

where d_{th} can be interpreted as the distance between the typical user and the limit separating both propagation environments.

To compare the three models, a new performance metric is introduced. It is defined as the probability that the received power from a BS is higher than a threshold a.

$$\mathbb{P}_{P_R} = \mathbb{P}\left[P_R > a\right] \tag{6.4}$$

where the expression of the received power P_R is obtained from Definition 3.2. For a single-slope path-loss function :

$$P_R(r) = P r^{-\alpha} |h|^2 \tag{6.5}$$

For a dual slope path-loss function :

$$P_R(r) = \begin{cases} P r^{-\alpha_0} |h|^2, & r \leq d_{th} \\ P d_{th}^{\alpha_1 - \alpha_0} r^{-\alpha_1} |h|^2, & r > d_{th} \end{cases} \tag{6.6}$$

As in the other chapters, the parameter κ and factor $1/4\pi$ are not taken into account.

Considering a HPPP with a density λ and a unit transmission power, and assuming a DAR, the performance metric is expressed as follows:

Proposition 6.1 ($\mathbb{P}_{P_R}$ - Single and Dual-slope Path-Loss Functionw)

The probability that the received power from the nearest BS to the origin in a HPPP is higher than a threshold a is given by:

For a single slope path-loss function,

$$\mathbb{P}_{P_R} = \int_0^\infty 2\pi\lambda r \exp\left(-\pi\lambda r^2 - ar^\alpha\right) dr, \quad \text{with} \quad \alpha = \{\alpha_0, \alpha_1\} \tag{6.7}$$

For a dual slope path-loss function,

$$\begin{aligned} \mathbb{P}_{P_R} = &\int_0^R 2\pi\lambda r \exp\left(-\pi\lambda r^2 - ar^{\alpha_0}\right) dr \\ &+ \int_R^\infty 2\pi\lambda r \exp\left(-\pi\lambda r^2 - ad_{th}^{-\alpha_1+\alpha_0} r^{\alpha_1}\right) dr \end{aligned} \tag{6.8}$$

Proof : see Appendix A.2

Numerical Results

To compare **model 1**, **model 2** and the hybrid model, the impact of distance d_{th} on $\mathbb{P}_{P_R}$ is analyzed for two densities λ. Curves shown in Figures 6.3 are obtained from expressions (6.7) and (6.8) for a PLE α_0 higher than α_1. The hybrid model is evaluated for three distances d_{th}, $(100, 500, 1500)[m]$. Two HPPPs with densities $(5 * 10^{-9}, 5 * 10^{-8})[BS/m^2]$ are considered for the numerical results. These HPPPs can also be characterized by the average distance of their nearest BS to the origin, $(7071, 2236)[m]$.

In Figure (a), for a relatively small distance $d_{th} = 100[m]$, neither the single slope model with the PLE α_0 nor α_1 provide a better approximation of the dual slope function. Once the distance d_{th} gets higher, the single slope function with PLE α_0 is closer to the hybrid model. In Figure (c), the same HPPP is considered but the difference of path-loss between both mediums is reduced. One can observe that the results are similar to Figure (a). These observations show that even if the signal propagates over a higher distance in a less lossy medium (α_1), the attenuation is dominated by the highest PLE (α_0). In Figure (b), by decreasing the mean distance to the BS and for same distances d_{th}, the single slope function with the PLE α_0 gets even closer to the hybrid model. A result that sounds logical.

To conclude this section, let us apply these observations to the 2-tiers example presented in the introduction. When the user is located in urban area, **model 2** will provide a better approximation to the real path-loss than **model 1** for the interfering signals. Indeed, **model 2** states that the PLE of the interference depends on the location of the user. In that case, for an urban area, the PLE is the highest. However, when the user is located in rural area, it is the opposite. **Model 1** is a better approximation. In the rest of this chapter, the preference is given to **model 2** because it leads to closed-form expressions.

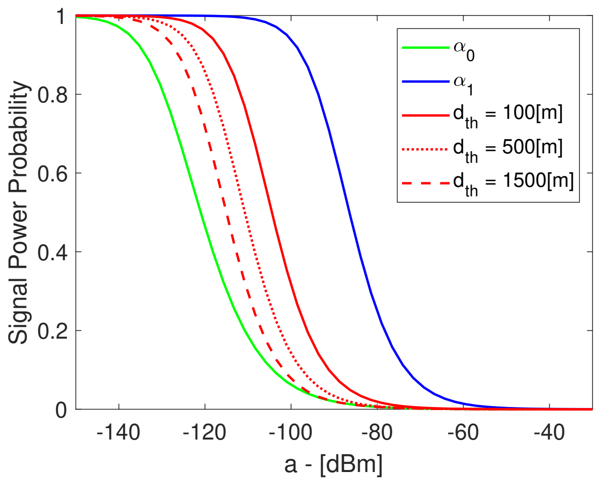

(a) $\lambda = 5 * 10^{-9}[BS/m^2]$, $(\alpha_0, \alpha_1) = (3.9, 3)$.

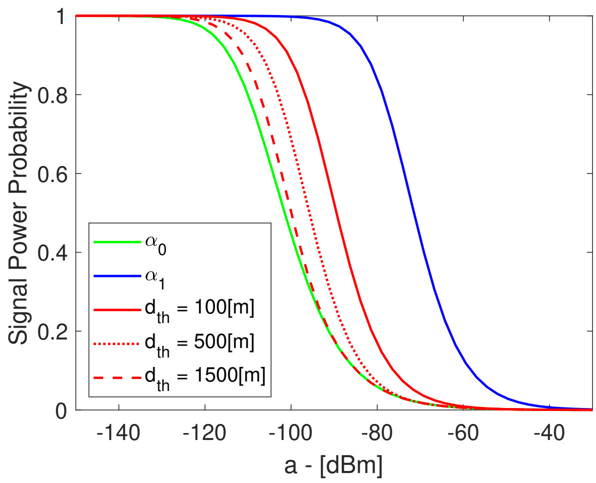

(b) $\lambda = 5 * 10^{-8}[BS/m^2]$, $(\alpha_0, \alpha_1) = (3.9, 3)$.

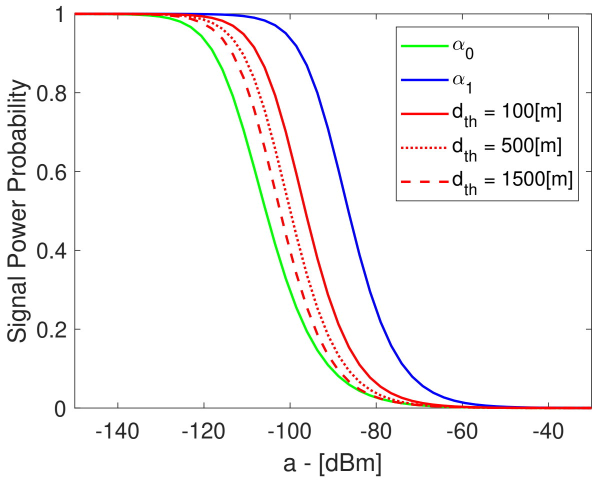

(c) $\lambda = 5 * 10^{-9}[BS/m^2]$, $(\alpha_0, \alpha_1) = (3.5, 3)$.

Figure 6.3: $\mathbb{P}_{P_R}$: blue and green curves correspond to (6.7), and red to (6.8)

6.2 Performance Metrics

In this chapter, the performance metrics are no longer defined for the entire HetNet but per tier, assuming the typical user is served by a given tier. The framework is the same as developed in section 5.1, based on the high SIR assumption and PAR. The rule for the PLEs follows **model 2**. The expressions of the CP and JPCE per tier are in closed-form. Even if the analysis focuses on a 2TN, the expressions are derived for a KTN.

Proposition 6.2 (Coverage Probability k^{th}-tier)

For $\theta > 1$, assuming the typical user is served by the k^{th}-tier in a KTN, and assuming a PAR and **model 2** for the PLEs, the CP is given by:

$$\begin{aligned}\mathbb{P}_{\mathrm{cv,k}}(\theta; k) &= \mathbb{P}\left[\bigcup_{r_{i,k}\in\boldsymbol{\Phi}_{\mathbf{k}}} \mathrm{SIR}(r_{i,k}) > \theta\right] \\ &= \frac{\theta^{-2/\alpha_k}\alpha_k \sin\left(\frac{2\pi}{\alpha_k}\right)\lambda_k P_k^{2/\alpha_k}}{2\pi\sum_{i=1}^{K}\lambda_i P_i^{2/\alpha_k}}\end{aligned} \tag{6.9}$$

Proof: from the proof of Proposition 5.1

Proposition 6.3 (Joint Probability of Coverage and Exposure k^{th}-tier)

For $\theta > 1$, assuming the typical user is served by the k^{th}-tier in a KTN, assuming a PAR, **model 2** for the PLEs and under the high SIR assumption, the JPCE is given by:

$$\begin{aligned}\mathbb{F}_k(\theta, \theta'; k) &= \mathbb{P}\left[\bigcup_{r_{i,k}\in\boldsymbol{\Phi}_{\mathbf{k}}} (\mathrm{SIR}(r_{i,k}) > \theta, \mathrm{EXPO}(r_{i,k}) < \theta')\right] \\ &= \frac{\theta^{-2/\alpha_k}\alpha_k \sin\left(\frac{2\pi}{\alpha_k}\right)\lambda_k P_k^{2/\alpha_k}}{2\pi\sum_{i=1}^{K}\lambda_i P_i^{2/\alpha_k}} - \frac{2\pi\lambda_k P_k^{2/\alpha_k}\Gamma(\frac{2}{\alpha_k})}{\alpha_k\theta'^{2/\alpha_k}}\end{aligned} \tag{6.10}$$

Proof: from the proof of Proposition 5.2

6.3 Constraints

The constraints defined for a tier addition differ from the general network deployment. The constraint on the MRP is now applied per tier and the constraints on the MFLs are no longer used. New constraints on the coverage and exposure are introduced to ensure a QoS and limit the exposure in the network despite its expansion. The formulation of the MRP, EP and CP constraints follows from Propositions 5.3 and 6.2.

Proposition 6.4 (Constraints $c_{1,i}$: MRPs)

The constraints on the MRPs in a KTN are defined as follows:

$$\mathbb{P}\left[\mathcal{S}_k < \delta\right] < \epsilon, \quad 0 < \epsilon < 1, \quad \forall k \in \{1, ..., K\}$$

$$\text{expressed as:} \quad \lambda_k P_k^{2/\alpha_k} > \epsilon'_k \tag{6.11}$$

$$\text{where} \quad \epsilon'_k = \frac{\alpha_k \delta^{2/\alpha_k} \log \frac{1}{\epsilon}}{2\pi\Gamma(\frac{2}{\alpha_k})} \tag{6.12}$$

Proposition 6.5 (Constraints $c_{2,i}$: CPs)

Assuming the typical user is served by the k^{th}-tier in a KTN, the constraints on the CPs are defined as follows:

$$\mathbb{P}_{\mathrm{cv,i}}(\theta; i) > \eta_i, \quad \eta_i < \frac{\theta^{-2/\alpha_i} \alpha_i \sin\left(\frac{2\pi}{\alpha_i}\right)}{2\pi}, \quad \forall k \in \{1, ..., K\}, \quad i \neq k$$

$$\text{where} \quad \mathbb{P}_{\mathrm{cv,i}} = \frac{\theta^{-2/\alpha_i} \alpha_i \sin\left(\frac{2\pi}{\alpha_i}\right) \lambda_i P_i^{2/\alpha_i}}{2\pi \sum_{j=1}^{K} \lambda_j P_j^{2/\alpha_i}} \tag{6.13}$$

Proposition 6.6 (Constraints $c_{3,i}$: EPs)

Assuming the typical user is served by the k^{th}-tier in a KTN and under the high SIR assumption, the constraints on the EPs are defined as follows:

$$\mathbb{P}\left[\mathcal{S}_k < \theta'\right] > \epsilon, \quad 0 < \epsilon < 1, \quad \forall k \in \{1, ..., K\}, \quad i \neq k$$

$$\text{expressed as:} \quad \lambda_k P_k^{2/\alpha_k} < \epsilon'_{\theta',k} \tag{6.14}$$

$$\text{where} \quad \epsilon'_{\theta',k} = \frac{\alpha_k \theta'^{2/\alpha_k} \log \frac{1}{\epsilon}}{2\pi\Gamma(\frac{2}{\alpha_k})} \tag{6.15}$$

6.4 Optimization Problem 2: Tier Densities and Transmission Powers

Even if the optimization is on a tier addition, it is considered that all the tier densities and transmission powers can be completely controlled. This leads to a more general formulation and allows to understand the interactions between the tiers.

In this section, a general formulation of a network expansion optimization on the densities is first introduced for a KTN. Then, the problem is solved for the special case of a 2TN. Depending on the parameters, different optimal solutions can be derived and are in closed-form. From this optimization on the densities, a second problem on the transmission powers can be introduced in order to further maximize the JPCE. An inverted formulation of the problem i.e. a first optimization on the transmission powers and then, on the densities, leads exactly to the same solution and is detailed in Appendix B.1.1.

For a 2TN, the analysis focuses on the specific case in which $\alpha_\mathbf{2} > \alpha_\mathbf{1}$ and $k = 2$. One can interpret this as a second tier deployment in propagation environments with higher losses. With **model 2**, expression (6.10) provides a better approximation to the real JPCE. However, the constraint on the CP in the first tier is a lower bound. This PLE choice is made to work with a the most accurate objective function.

6.4.1 K-tiers Network - Optimization Problem Formulation

Let us formulate optimization problem 2 (**P2**) for a KTN. The objective function of **P2** is defined as follows:

$$\begin{aligned}\mathcal{F}(\{\lambda_i\}_{i=1}^{K};\theta,\theta',k) &= \mathbb{F}_k(\theta,\theta';k)\\ &= \frac{\theta^{-2/\alpha_k}\alpha_k \sin\left(\frac{2\pi}{\alpha_k}\right)\lambda_k P_k^{2/\alpha_k}}{2\pi\sum_{i=1}^{K}\lambda_i P_i^{2/\alpha_k}} - \frac{2\pi\lambda_k P_k^{2/\alpha_k}\Gamma(\frac{2}{\alpha_k})}{\alpha_k \theta'^{2/\alpha_k}} \qquad (6.16)\end{aligned}$$

The tier densities are optimized in order the maximize the JPCE in the k^{th}-tier under constraints on the MRPs, CPs and EPs.

$$\max_{\{\lambda_i\}_{i=1}^K} \mathcal{F}(\{\lambda_i\}_{i=1}^K; \theta, \theta', k)$$

$$\begin{aligned}
\text{such that} \quad & c_{1,i}: && \lambda_i P_i^{2/\alpha_i} > \epsilon_i', \quad \forall i \in 1, ..., K \\
& c_{2,i}: && \mathbb{P}_{\mathrm{cv,i}} > \eta_i, \quad \forall i \in 1, ..., K, \quad i \neq k \\
& c_{3,i}: && \lambda_i P_i^{2/\alpha_i} < \epsilon_{\theta',i}', \quad \forall i \in 1, ..., K, \quad i \neq k \\
& c_{4,i}: && \lambda_i \geq 0
\end{aligned}$$

6.4.2 2-tiers Network - Analytical Solution

For a 2TN, **P2** is reduced to this formulation.

Definition 6.2 (P2 - 2-tiers Network)

$$\max_{\{\lambda_i\}_{i=1}^2} \frac{C(\alpha_2, \theta)\lambda_2 P_2^{2/\alpha_2}}{\lambda_1 P_1^{2/\alpha_2} + \lambda_2 P_2^{2/\alpha_2}} - D(\alpha_2, \theta')\lambda_2 P_2^{2/\alpha_2} \tag{6.17}$$

$$\begin{aligned}
\text{such that} \quad & c_{1,1}: && \lambda_1 P_1^{2/\alpha_1} > \epsilon_1' \\
& c_{1,2}: && \lambda_2 P_2^{2/\alpha_2} > \epsilon_2' \\
& c_{2,1}: && \lambda_1 P_1^{2/\alpha_1} \left(C(\alpha_1, \theta) - \eta_1\right) - \lambda_2 P_2^{2/\alpha_1} \eta_1 > 0 \\
& c_{3,1}: && \lambda_1 P_1^{2/\alpha_1} < \epsilon_{\theta',1}' \\
& c_{4,i}: && \lambda_i \geq 0, \quad \forall i \in \{1, 2\}
\end{aligned}$$

$$\text{where} \quad C(\alpha, \theta) = \frac{\theta^{-2/\alpha} \alpha \sin\left(\frac{2\pi}{\alpha}\right)}{2\pi} \quad \text{and} \quad D(\alpha, \theta') = \frac{2\pi\Gamma(\frac{2}{\alpha})}{\alpha \theta'^{2/\alpha}}$$

Let $\mathcal{R}$ denote the feasible region of **P2**:

$$\begin{aligned}
\mathcal{R} = \Big\{ & (\lambda_1, \lambda_2) \in \mathbb{R}_+^2 | \lambda_1 P_1^{2/\alpha_1} > \epsilon_1', \lambda_2 P_2^{2/\alpha_2} > \epsilon_2', \\
& \lambda_1 P_1^{2/\alpha_1} \left(C(\alpha_1, \theta) - \eta_1\right) - \lambda_2 P_2^{2/\alpha_1} \eta_1 > 0, \\
& \lambda_1 P_1^{2/\alpha_1} < \epsilon_{\theta',1}' \Big\}
\end{aligned} \tag{6.18}$$

It is assumed that the parameters are chosen such that the space $\mathcal{R}$ is nonempty. This assumption especially relies on $\epsilon_{\theta',1}'$.

In order to derive the optimal solution, both terms of objective function (6.17) can be analyzed separately. For a 2TN, the first term, the CP, can be rewritten as a function of λ_2/λ_1.

$$\mathbb{P}_{\mathrm{cv},2}(\theta) = \frac{C(\alpha_2,\theta)P_2^{2/\alpha_2}}{\frac{\lambda_1}{\lambda_2}P_1^{2/\alpha_2} + P_2^{2/\alpha_2}} \tag{6.19}$$

Therefore, the set of optimal solutions maximizing the CP is given by:

$$(\lambda_1^*, \lambda_2^*) = \arg\max_{(\lambda_1,\lambda_2)\in\mathcal{R}} \frac{\lambda_2}{\lambda_1} \tag{6.20}$$

Let us now consider the second term. The set of optimal solutions maximizing $-D(\alpha_2,\theta')\lambda_2 P_2^{2/\alpha_2}$ is given by:

$$(\lambda_1^*, \lambda_2^*) = \arg\min_{(\lambda_1,\lambda_2)\in\mathcal{R}} \lambda_2 \tag{6.21}$$

Let us now analyse the feasible region. From (6.18), there are two possible configurations as illustrated in Figure 6.4. First, the edges of $\mathcal{R}$ correspond to the lines defined by setting equalities in the constraints $c_{1,2}$ and $c_{2,1}$. The feasible region is in the first configuration if:

$$P_2^{2/\alpha_1 - 2/\alpha_2} > \frac{\epsilon_1'}{\epsilon_2'} \frac{(C(\alpha_1,\theta) - \eta_1)}{\eta_1} \tag{6.22}$$

This inequality is derived by comparing the intersection ($c_{1,2}$, $c_{2,1}$) with $c_{1,1}$. In the second configuration, the edges are defined by setting equalities in the first three constraints. Let us derive the expressions of the optimal solutions for both configurations.

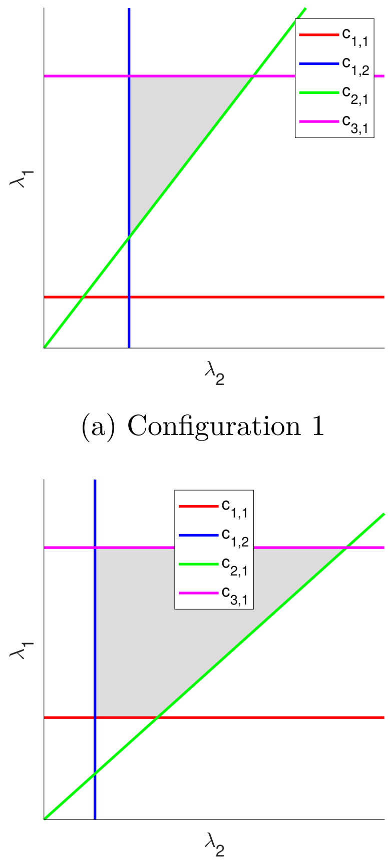

(a) Configuration 1

(b) Configuration 2

Figure 6.4: **P2** - Feasible Region

In the first case, one can observe that the line defining the constraint $c_{2,1}$ is the set of points maximizing the first term of expression (6.17) in $\mathcal{R}$. The solution of expression (6.21) is also straightforward, the line defined by the constraint $c_{1,2}$. By combining (6.20) and (6.21), the optimal solution to **P2** is defined by the intersection $(c_{1,2}, c_{2,1})$ for this specific configuration.

For the second configuration, let us first consider any line parallel to $c_{1,2}$ and included between the intersections $(c_{1,1}, c_{1,2})$ and $(c_{1,1}, c_{2,1})$ (see Fig.6.5(a)). For any point (λ_1, λ_2) on this line, the second term of objective function (6.17) assumes the same value. Consequently, reminding the maximization of (6.17), the optimal solution is located at the intersection with $c_{1,1}$ because it is the point maximizing the ratio λ_2/λ_1 on this line and in the feasible region. Let us now consider the constraint $c_{2,1}$ (see Fig.6.5(b)). Any point on this line maximizes the first term of objective function (6.17) in the feasible region. Moreover, the point maximizing the second term of (6.17) in $\mathcal{R}$ and on $c_{2,1}$ is the intersection with $c_{1,1}$. As a result, for the second configuration, the set of optimal solutions is located on the constraint $c_{1,1}$ and delimited by the intersections $(c_{1,1}, c_{1,2})$ and $(c_{1,1}, c_{2,1})$. One can then distinguish three cases. The solution is the intersection $(c_{1,1}, c_{1,2})$, $(c_{1,1}, c_{2,1})$ or any point between both intersections.

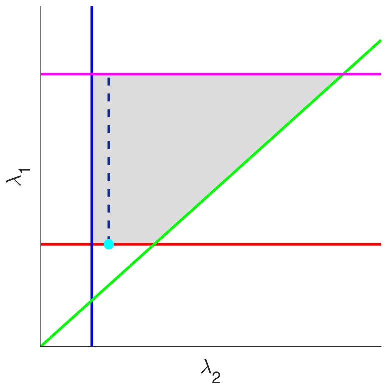

(a) Case 1

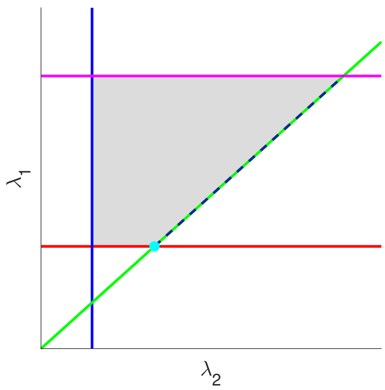

(b) Case 2

Figure 6.5: **P2** - Configuration 2 : Solution Visualizations

Finally, let us combine these analyses and propose a complete formulation of the optimal solutions. Figure 6.6 shows an illustration of the optimal solutions.

Proposition 6.7 (P2 - Analytical Solutions $(\lambda_1^*, \lambda_2^*)$)

If the feasible region is in the first configuration, the optimal solution is given by:

$$(\lambda_1^*, \lambda_2^*) = \left(\frac{\epsilon_2'}{C(\alpha,\theta,\eta_1)} \frac{P_2^{2/\alpha_1 - 2/\alpha_2}}{P_1^{2/\alpha_1}}, \frac{\epsilon_2'}{P_2^{2/\alpha_2}} \right) \quad \textbf{Sol.1} \tag{6.23}$$

If the feasible region is in the second configuration, there are three possible analytical solutions. If the solution is located on the intersection $(c_{1,1}, c_{1,2})$, it is given by:

$$(\lambda_1^*, \lambda_2^*) = \left(\frac{\epsilon_1'}{P_1^{2/\alpha_1}}, \frac{\epsilon_2'}{P_2^{2/\alpha_2}} \right) \quad \textbf{Sol.2} \tag{6.24}$$

If the solution is located on the intersection $(c_{1,1}, c_{2,1})$, it is given by:

$$(\lambda_1^*, \lambda_2^*) = \left(\frac{\epsilon_1'}{P_1^{2/\alpha_1}}, \frac{\epsilon_1' C(\alpha,\theta,\eta_1)}{P_2^{2/\alpha_1}} \right) \quad \textbf{Sol.3} \tag{6.25}$$

Otherwise, the solution is located between both intersections and is given by:

$$(\lambda_1^*, \lambda_2^*) = \left(\frac{\epsilon_1'}{P_1^{2/\alpha_1}}, \frac{\left(\frac{C(\alpha_2,\theta) P_1^{2/\alpha_2 - 2/\alpha_1} \epsilon_1'}{D(\alpha_2,\theta')} \right)^{1/2} - \epsilon_1' P_1^{2/\alpha_2 - 2/\alpha_1}}{P_2^{2/\alpha_2}} \right) \quad \textbf{Sol.4} \tag{6.26}$$

$$\text{where} \quad C(\alpha,\theta,\eta_1) = \frac{(C(\alpha,\theta) - \eta_1)}{\eta_1}$$

Expression (6.26) is derived by setting the derivative of the objective function to 0.

For the rest of this chapter, only the first configuration is considered. In the final section, a discussion on this topic is provided. In the next sub-section, **Sol.1** is further analysed. By inserting expression (6.23) into the objective function, an additional optimization problem can be introduced.

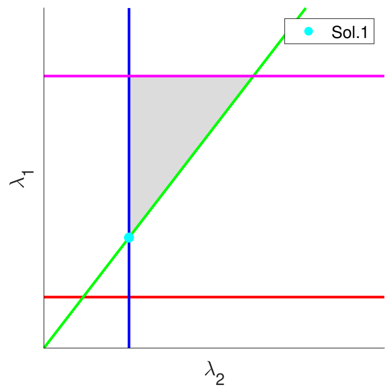

(a) Configuration 1

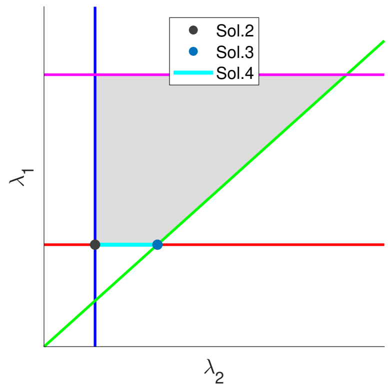

(b) Configuration 2

Figure 6.6: **P2** - Feasible Region and Optimal Solutions

Optimization Problem 2.1: Tier Transmission Powers

Let us evaluate objective function (6.17) at **Sol.1** given by (6.23).

Proposition 6.8 ($\mathcal{F}(\lambda_1^*, \lambda_2^*; \theta, \theta')$ - Sol.1)

The objective function of **P2** evaluated at **Sol.1** is given by:

$$\mathcal{F}(\lambda_1^*, \lambda_2^*; \theta, \theta') = \frac{C(\alpha_2, \theta)}{C(\alpha_1, \theta, \eta_1)^{-1} \left(\frac{P_2}{P_1}\right)^{2/\alpha_1 - 2/\alpha_2} + 1} - D(\alpha_2, \theta')\epsilon_2' \tag{6.27}$$

One can formulate an additional optimization problem on the transmission powers, referenced as optimization problem 2.1 (**P2.1**).

Proposition 6.9 (P2.1 - 2-tiers Network)

$$\max_{\{P_i\}_{i=1}^{2}} \frac{C(\alpha_2,\theta)}{C(\alpha_2,\theta,\eta_1)^{-1}\left(\frac{P_2}{P_1}\right)^{2/\alpha_1-2/\alpha_2}+1} - D(\alpha_2,\theta')\epsilon_2' \tag{6.28}$$

$$\begin{aligned}
\text{such that}\quad & c_{1,1}: && \lambda_1^* P_1^{2/\alpha_1} > \epsilon_1' \\
& c_{1,2}: && \lambda_2^* P_2^{2/\alpha_2} > \epsilon_2' \\
& c_{2,1}: && \lambda_1^* P_1^{2/\alpha_1}\left(C(\alpha_1,\theta)-\eta_1\right) - \lambda_2^* P_2^{2/\alpha_1}\eta_1 > 0 \\
& c_{3,1}: && \lambda_1^* P_1^{2/\alpha_1} < \epsilon_{\theta',1}' \\
& c_4: && P_2^{2/\alpha_1-2/\alpha_2} > \frac{\epsilon_1'}{\epsilon_2'} C(\alpha_1,\theta,\eta_1) \\
& c_{5,i}: && P_i \geq 0, \quad \forall i \in \{1,2\}
\end{aligned}$$

The constraint c_4 is the condition to be in configuration 1 (6.22). By substituting (6.23) in the expressions of the constraints, the feasible region denoted by $\mathcal{R}$ is defined as follows:

$$\begin{aligned}
\mathcal{R} = \Big\{ & (P_1,P_2) \in \mathbb{R}_+^2 \,|\, P_2^{2/\alpha_1-2/\alpha_2} > \frac{\epsilon_1'}{\epsilon_2'} C(\alpha_1,\theta',\eta_1), \\
& P_2^{2/\alpha_1-2/\alpha_2} < \frac{\epsilon_{1,\theta'}'}{\epsilon_2'} C(\alpha_1,\theta,\eta_1) \Big\}
\end{aligned} \tag{6.29}$$

Figure 6.7 shows a visualization of the feasible region.

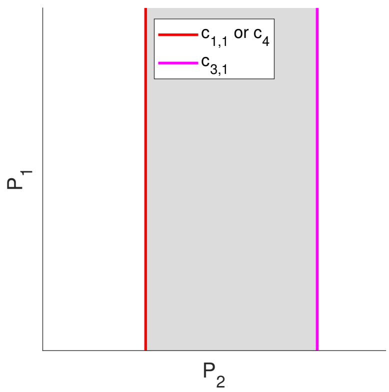

Figure 6.7: **P2.1** - Feasible Region

Assuming $\alpha_2 > \alpha_1$, one can deduce that the optimal solution to **P2.1** is expressed as follows:

$$(P_1^*, P_2^*) = \underset{(P_1,P_2)\in\mathcal{R}}{\arg\max} \frac{P_1}{P_2} \tag{6.30}$$

As mentioned in the introduction of this chapter, it leads to a non-realistic final solution with P_1^* that tends to infinity and λ_1^* equals to zero.

Mathematical Interpretation

As the optimal solution to **P2** is on the constraint $c_{1,2}$ (i.e. the minimum exposure in the second tier), **P2.1** is only about the CP and tends to a maximization of the ratio P_1/P_2. This results may seem counter intuitive. Indeed, from expression (6.19), one can deduce that the probability decreases with this ratio. To understand this behavior, let us analyse the impact of P_1/P_2 on the constraint $c_{2,1}$. From equation (6.9), the coverage probability in tier 1 can be expressed as a function of the transmission power ratio.

$$\mathbb{P}_{\mathrm{cv},1}(\theta) = \frac{C(\alpha_1,\theta)\lambda_1}{\lambda_1 + \lambda_2 \left(\frac{P_2}{P_1}\right)^{2/\alpha_1}} \tag{6.31}$$

The probability increases with the ratio P_1/P_2. One can therefore interpret **P2.1** as a relaxation of the constraint $c_{2,1}$, as illustrated by the arrow in Figure 6.8. Due to the exponent $2/\alpha_2 < 1$, the coverage dependency towards the density ratio is higher than that of the transmission power in the second tier. This observation demonstrates the objective of **P2.1**: increase P_1/P_2 in order to further increase λ_2/λ_1 and therefore, the CP in tier 2 thanks to a relaxation of the constraint $c_{2,1}$.

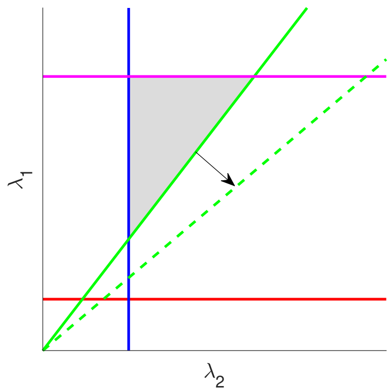

Figure 6.8: **P2.1** - **P2** Constraints

6.5 Numerical Results and Discussions

In this final section, the different optimal solutions and the feasible regions of **P2** are discussed and interpreted. Finally, the impact of the PLEs on the optimal solution and the JCPE is analysed.

6.5.1 Optimization on the Tier Densities: Discussion

To solve the optimization on the tier densities, two configurations are considered for the feasible region. Both configurations lead to different optimal solutions and interpretations.

In the first configuration, there is an intersection between the set of optimal solutions that maximize the coverage and minimize the exposure in the feasible region. Therefore, the configuration is such that both coverage and exposure can be optimized simultaneously.

For the second configuration, this observation is no longer valid. Indeed, the optimisation of the coverage is at the expense of the exposure, and inversely. Depending on parameters, the optimal solution is located somewhere between the intersections $(c_{1,1}, c_{1,2})$ and $(c_{1,1}, c_{2,1})$. **Sol.2** maximizes the EP and **Sol.3**, the CP in the second tier. **Sol.4** allows to highlight an inconvenient of the JPCE choice as the objective function for the optimization. As mentioned several times in this work, this performance metric is the sum of two terms, the CP and a second related to the EP. Consequently, depending on parameters and especially, θ, θ', the optimization of the joint probability can lead to the maximization of one of the two quantities and not both simultaneously. Figure 6.9 illustrates this discussion. **Sol.4** is plotted with respect to the threshold θ and for different θ'. The numerical values of the optimal density λ_2^* are not relevant. The interest of this figure is to show the behavior of expression 6.26. It is worth to mention that this expression is not necessarily the solution to **P2**. It expresses the optimal density λ_2^* on the constraint $c_{1,1}$ no matter the feasible region. Two specific behaviors can be observed. First, λ_2^* decreases with θ' which is coherent. However, by increasing θ, the optimal density decreases which is not an expected result. This can be explained thanks to the mathematical expression of the JPCE. Increasing θ decreases the CP, consequently, the exposure term dominates in the optimization.

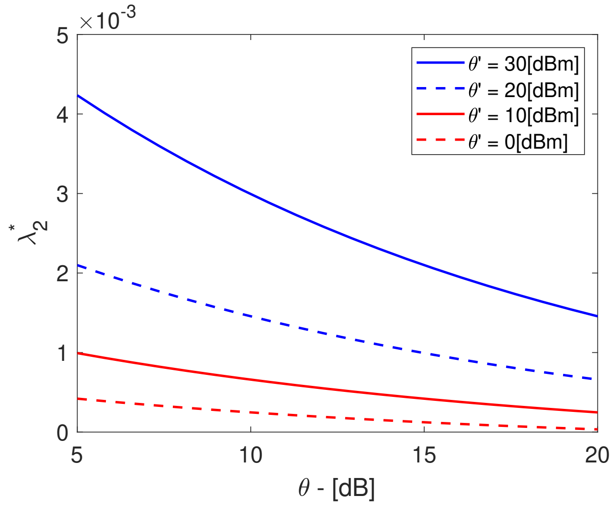

Figure 6.9: **P2**, **Sol.4** - Impact of θ and θ': $\epsilon = 0.1$, $\delta = -20[dBm]$, $(P_1, P_2) = (60, 30)[dBm]$, $(\alpha_1, \alpha_2) = (3, 3.5)$.

This observation shows the limits of the optimization problem introduced in this chapter. In order to jointly optimize both coverage and exposure in a HetNet, a new performance metrics needs then to be define. However, it does not mean that the results obtained in this chapter can not be used. The first configuration shows that a joint optimization is possible and this will be further analysed in this section.

6.5.2 Feasible Region Configurations: Discussion

In this chapter, the optimization mainly focuses on the first configuration for two reasons. First, the second configuration leads to a questionable final result as explained previously. Second, a tier addition in the network is done at the expense of the coverage in the other tiers and the first configuration is the most constraining with respect to the CP in tier 1. Figure 6.10 shows the impact of the parameter η_1 on the constraints. This parameter can express a percentage of the maximum CP in the first tier, $C(\alpha_1, \theta)$.

$$\frac{\lambda_1 P_1^{2/\alpha_1}}{\lambda_1 P_1^{2/\alpha_1} + \lambda_2 P_2^{2/\alpha_1}} > \frac{\eta_1}{C(\alpha_1, \theta)}[\%]$$

Increasing η_1 and therefore, the constraint on the CP in tier 1 tends to the first configuration.

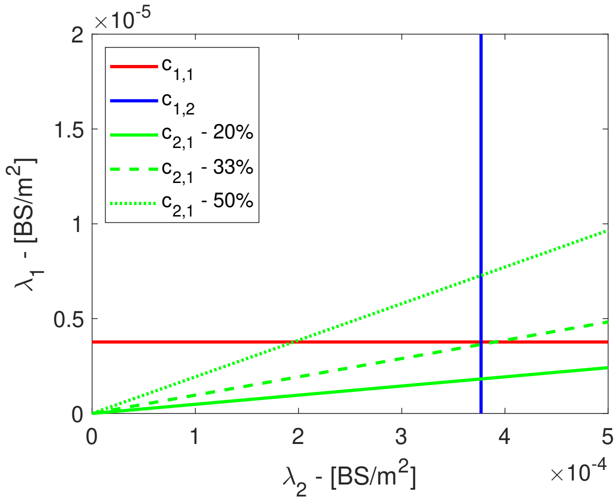

Figure 6.10: **P2** Constraints - Impact of η_1: $\theta = 10[dB]$, $\epsilon = 0.1$, $\delta = -20[dBm]$, $(P_1, P_2) = (60, 30)[dBm]$, $(\alpha_1, \alpha_2) = (3, 3.5)$.

6.5.3 Network Expansion - Optimal Solution: Interpretation

It is worth to mention that the optimization of the JPCE in the second tier is mainly about the CP. This comes from the first configuration of the feasible region. As the optimal solution is on the constraint $c_{1,2}$, a minimum of exposure is ensured in the second tier. Therefore, **P2.1** is only focused on the coverage. It is also interesting to observe that the nature of the problem does not involve the constraint $c_{3,1}$ in the developments. In fact, a maximization of the CP in the second tier implies a maximization of the EP in the first tier.

Despite all the constraints, the optimal solutions λ_1^*, λ_2^*, P_1^* and P_2^* obtained from **P2.1** are not realistic (i.e. $P_1^* = \infty$ and $\lambda_1^* = 0$). Some practical constraints on the transmission powers should be defined to avoid this trivial solution. Nevertheless, from expression 6.23, an interesting relationship between the ratios P_1^*/P_2^* and λ_1^*/λ_2^* can be established. The following Proposition provides all the useful expressions obtained from **P2**.

Proposition 6.10 (Network Expansion - Optimal Relationships)

For a 2TN expansion, the optimal relationship between the tier densities and transmission powers is given by:

$$\frac{P_1^*}{P_2^*} = C(\alpha_1, \theta, \eta_1)^{-\alpha_1/2} \left(\frac{\lambda_2^*}{\lambda_1^*}\right)^{\alpha_1/2} \tag{6.32}$$

with

$$(\lambda_1^*, \lambda_2^*) = \left(\epsilon_2' C(\alpha_1, \theta, \eta_1)^{-1} \frac{P_2^{*2/\alpha_1 - 2/\alpha_2}}{P_1^{*2/\alpha_1}}, \frac{\epsilon_2'}{P_2^{*2/\alpha_2}}\right) \tag{6.33}$$

The objective function evaluated at $(\lambda_1^*, \lambda_2^*)$ or equivalently (P_1^*, P_2^*) is given by:

$$\mathcal{F}(\lambda_1^*, \lambda_2^*; \theta, \theta') = \frac{C(\alpha_2, \theta)}{C(\alpha_1, \theta, \eta_1)^{-1} \left(\frac{P_2^*}{P_1^*}\right)^{2/\alpha_1 - 2/\alpha_2} + 1} - D(\alpha_2, \theta')\epsilon_2' \tag{6.34}$$

$$\mathcal{F}(P_1^*, P_2^*; \theta, \theta') = \frac{C(\alpha_2, \theta)}{C(\alpha_2, \theta, \eta_1)^{-\alpha_1/\alpha_2} \left(\frac{\lambda_2^*}{\lambda_1^*}\right)^{\alpha_1/\alpha_2 - 1} + 1} - D(\alpha_2, \theta')\epsilon_2' \tag{6.35}$$

Given relationship (6.32), the network expansion optimization is reduced to the maximization of expressions (6.34) and (6.35) with respect to the ratio P_1^*/P_2^* or λ_1^*/λ_2^* (as proposed in **P2.1**). Furthermore, this relationship reveals that the optimal ratios must be inversely proportional. For a 2TN with $\alpha_2 > \alpha_1$, **P2** and **P2.1** show that the second tier should be deployed with the highest density and smallest transmission power, at the opposite of the first tier, i.e. low density and high transmission power.

Proposition 6.10 provides a general interpretation of the network expansion optimization. When the tiers experience different conditions of propagation, it demonstrates the necessity to differentiate the tiers. By comparing expressions of $\mathbb{P}_{\text{cv},1}$ and $\mathbb{P}_{\text{cv},2}$, a network expansion can not be done without degrading the performances in the initial tier. Despite this observation, the optimization studied in this chapter highlights the fact that a maximum of performances can be extracted from a tier by adapting the network characteristics, λ_k, P_k.

6.5.4 Impact of the Path-Loss Exponents

In this last section, let us analyse the impact of the PLEs α_1 and α_2.

Figure 6.11 shows curves of expression (6.35) with respect to λ_2^*/λ_1^* for different PLEs. For a given ratio, the network performances are enhanced when the difference between the PLEs gets higher. Indeed, in Figure 6.11, it is assumed that $\alpha_2 > \alpha_1$ and the JPCE increases with α_2. The curve $(\alpha_1, \alpha_2) = (3, 3.3)$ shows a quick saturation of the performances with respect to the ratio. Therefore, differentiate the tiers by their density and transmission power is even more effective when the losses are highly different. Moreover, for a given required JPCE, the optimal ratio λ_2^*/λ_1^* needs to be increased when α_2 gets closer to α_1. One can intuitively interpret this result as follows. If the propagation conditions of the HetNet does not sufficiently differentiate the tiers, this differentiation must be done by their characteristics.

Figure 6.12 illustrates the impact of α_1 on relationship (6.32). No matter α_2, by increasing α_1, the differentiation of the tiers is further emphasized. Hence, if the initial tier experiences high losses, one should consider a new tier with very different features to expand the network.

In this chapter, the interpretation is covered for $\alpha_2 > \alpha_1$. For that case, **P2** and **P2.1** demonstrate that the second tier should be deployed with a high density and small transmission power, at the opposite of the first tier. The curves in Figure 6.11 proof and illustrate this result. Nevertheless, all the expressions in Proposition 6.10 are obtained for any couple of values (α_1, α_2). Figure 6.13 shows the same curves as in Figure 6.11 for $\alpha_2 < \alpha_1$ and with respect to λ_1^*/λ_2^*. From this curves, one can deduce that the network characteristics are inverted. The second tier should be deployed with the lowest density and highest transmission power, at the opposite of the first tier (i.e. high density and low transmission power). From this observation, a last conclusion can be drawn. The optimal solution to a network expansion is to deploy a tier with a maximum density and a transmission power inversely proportional in areas with higher losses. Consequently, a small density of BSs with high transmission power is preferred in the other tier.

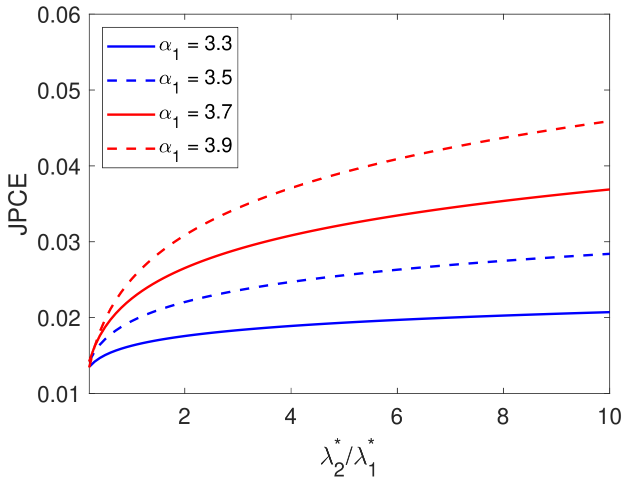

Figure 6.11: $\mathcal{F}(\frac{\lambda_2^*}{\lambda_1^*}; \theta, \theta')$ - Impact of (α_1, α_2): $\theta = 10[dB]$, $\theta' = 20[dBm]$, $\epsilon = 0.1$, $\delta = -20[dBm]$, $\alpha_1 = 3$, $\eta_1 = \frac{C(\alpha_1,\theta)}{1.5}$.

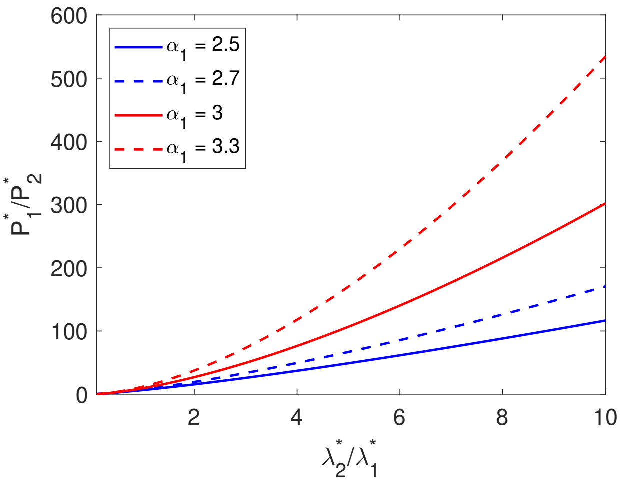

Figure 6.12: Optimal Relationship $\frac{P_1^*}{P_2^*}$, $\frac{\lambda_2^*}{\lambda_1^*}$ - Impact of α_1: $\theta = 20[dBm]$, $\delta = -20[dBm]$, $\eta_1 = \frac{C(\alpha_1,\theta)}{1.5}$.

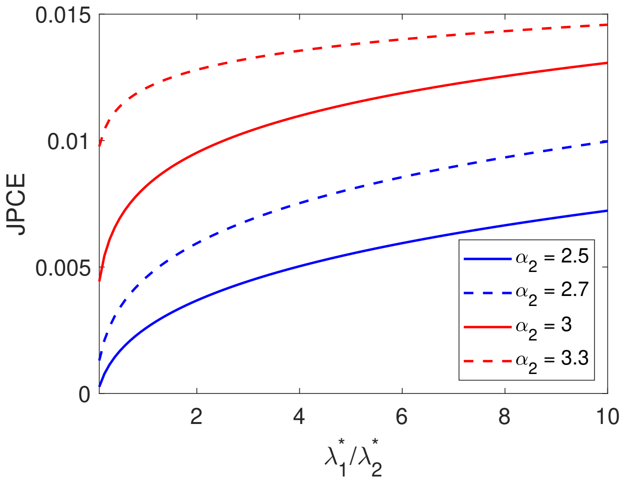

Figure 6.13: $\mathcal{F}(\frac{\lambda_1^*}{\lambda_2^*};\theta,\theta')$ - Impact of (α_1,α_2): $\theta = 10[dB]$, $\theta' = 20[dBm]$, $\epsilon = 0.1$, $\delta = -20[dBm]$, $\alpha_1 = 3.5$, $\eta_1 = \frac{C(\alpha_1,\theta)}{1.5}$.

Chapter 7

Conclusion

In this master's thesis, a general framework based on the Gil-Pelaez theorem has been developed for the JPCE in HetNets. Based on this performance metric, two joint optimizations of coverage and exposure have been introduced.

First, the Gil-Pelaez based model has been considered accurate for Rayleigh fading after validations with MC simulations. However, the validity of this model is limited down to sufficiently high exposure thresholds. Otherwise, the theoretical results assume negative values when the JPCE is null. The mathematical complexity of the Gil-Pelaez based model makes it difficult to understand the impact of parameters as the densities and transmission powers.

For the purpose of introducing solvable optimization problems, a second framework based on assumptions has been developed for the JPCE in HetNets. Its validity is limited to high SIRs but the assumptions allows to derive tractable models.

Next, a first optimization problem of a HetNet deployment has been introduced with a common path-loss. With identical conditions of wave propagation for all the tiers, the solution to this problem shows that a HomNet and a HetNet provide the same performances. Furthermore, a joint optimization on the densities and transmission powers does not improve the optimal JPCE. Moreover, due to the independence of the CP towards the tier densities and transmission powers, the optimal JPCE is obtained by minimising the exposure in the network i.e. minimizing the densities and powers.

Finally, a network expansion optimization has been introduced for the sake of analysing the behavior of a HetNet with different path-loss. This optimization highlights the interest of deploying HetNet and the necessity to differentiate the tiers. For a 2TN, one will then favor the deployment of micro BSs with a high density in areas with higher losses (e.g. urban) and provide coverage with macro BSs elsewhere (e.g. rural).

Some areas for improvement and further developments can be proposed for future studies in the field of SG based optimization of coverage and exposure in wireless networks:

- All the analysis has been made assuming Rayleigh fading. It might be interesting to include Ricean fading or Nakagami fading in the framework. One could suggest to differentiate the conditions of propagation in the HetNet with different path-loss and fading. Obviously, this will increase the mathematical complexity but the optimal solution can be computed numerically and compared to Rayleigh fading.
- In chapter 6, the optimization problem highlights the inconvenient of the JPCE as the objective function. Define a new performance metric adapted to the optimization should be considered. A conditional probability rather than a joint probability could be promising.
- The deployment strategy of a wireless network also depends on the density of UEs. This aspect has not been covered in this thesis. Future studies could include this parameters in the constraints or define a new performance metric combining coverage, exposure and the average rate per user.
- When analysing the exposure in a wireless network, the exposure to the UE in uplink transmissions should also be studied. For this purpose, a similar performance metric to downlink should be defined. In uplink, one can assimilate the exposure to the transmission power of the UE. Based on power control, a study in [21] derives a quasi closed-form expression for the CP in uplink.

Finally, in this master's thesis, a basis framework for the joint optimization of coverage and exposure has been introduced in the field of SG and an understanding of the optimal deployment strategy has been provided.

Appendices

Appendix A

Proofs

A.1 Lemma

Proof of Lemma 2.1 : *This proof is proposed in [19].* From the definition of c_i :

$$\begin{aligned} c_i &= \frac{a_i}{\sum_{j=1}^{n} a_j - a_i} \\ &\implies \frac{c_i}{1+c_i} = \frac{a_i}{\sum_{j=1}^{n} a_j} \\ &\implies \sum_{i=1}^{n} \frac{1}{\frac{1}{c_i}+1} = 1 \end{aligned} \tag{A.1}$$

The Lemma is first proven for $m = 1$ by contradiction. A.1 is satisfied if only one of the c_i's is greater than 1. Now assume that two c_i's are greater than one and without loss of generality, assume that they are c_1 and c_2. This implies $\frac{1}{c_1}$ and $\frac{1}{c_2}$ $\in [0,1]$. Therefore, $\frac{1}{\frac{1}{c_1}+1}$ and $\frac{1}{\frac{1}{c_2}+1}$ $\in [\frac{1}{2},1]$. Thus,

$$\begin{aligned} \sum_{i=1}^{n} \frac{1}{\frac{1}{c_i}+1} &= \sum_{i=1}^{2} \frac{1}{\frac{1}{c_i}+1} + \sum_{i=3}^{n} \frac{1}{\frac{1}{c_i}+1} \\ &> 1 + \sum_{i=3}^{n} \frac{1}{\frac{1}{c_i}+1} \end{aligned} \tag{A.2}$$

which is in contradiction with A.1. Since A.1 does not even hold for two c_i's greater than one, it proves that only one of the c_i's can be greater than one. Similarly for the case of general m, it is easy to observe that A.1 is trivially satisfied if at most m of the c_i's are greater than $\frac{1}{m}$. Now assume that $m+1$ c_i's are greater than $\frac{1}{m}$ and without loss of generality, assume that they are $c_1, c_2, ..., c_{m+1}$. Proceeding as in A.2,

$$\sum_{i=1}^{n} \frac{1}{\frac{1}{c_i}+1} > 1 + \sum_{i=m+2}^{n} \frac{1}{\frac{1}{c_i}+1}$$

which is in contradiction with A.1. Therefore, at most m c_i's can be greater than $\frac{1}{m}$.

A.2 Propositions

Proof of Proposition 2.1 : *This proof is proposed in [8].* Let $B(o,r)$ be the ball centred at the origin o and of radius r. The CCDF of D is derived as follows:

$$\begin{aligned} CCDF_D(r) &= \mathbb{P}\left[D \geq r\right] \\ &\overset{(b)}{=} \mathbb{P}\left[\mathbf{\Phi}(B(o,r)) = 0\right] \\ &\overset{(b)}{=} \exp\left(-\lambda |B(o,r)|\right) \\ &\overset{(c)}{=} \exp\left(-\lambda \pi r^2\right) \end{aligned} \tag{A.3}$$

which completes the proof. Step (a) follows from the definition of the void probability, (b) follows from the equation 2.1 and (c) from the area of a circle.

Proof of Proposition 4.2 : For a fixed serving distance r_0, $\mathcal{S}$ follows the distribution of the channel power gain. Step (a) follows from the definition of the CF of $|h|^2$.

$$\begin{aligned} \phi_{\mathcal{S}}(q; r_0) &= \mathbb{E}_{\mathcal{S}}\left[\exp\left(jq\mathcal{S}\right)\right]_{r_0} \\ &= \mathbb{E}_{|h|^2}\left[\exp\left(jqP|h|^2 r_0^{-\alpha}\right)\right]_{r_0} \\ &\overset{(a)}{=} \phi_{|h|^2}\left(qPr_0^{-\alpha}\right) \end{aligned}$$

which completes the proof.

Proof of Proposition 4.3 : For a fixed serving distance r_0, the expectation over $\mathcal{I}$ is obtained by taking the expectation over both HPPP and channel power gain. Step (a) comes from the definition of $\mathcal{I}$, and from the independence of the BS distribution in the HPPP and the independence of the channel power gains. (b) follows from the PGFL and the interference boundary $r_{\mathcal{I}} = r_0$, and (c) from the definition of the CF of $|h|^2$.

$$
\begin{aligned}
\phi_{\mathcal{I}}(q; r_0) &= \mathbb{E}_{\mathcal{I}}\left[\exp\left(jq\mathcal{I}\right)\right]_{r_0} \\
&\overset{(a)}{=} \mathbb{E}_{\mathbf{\Phi}/\mathcal{I}}\left[\prod_{r_i \in \mathbf{\Phi}/r_0} \mathbb{E}_{|h|^2}\left[\exp\left(jqP|h|^2 r_i^{-\alpha}\right)\right]\right]_{r_0} \\
&\overset{(b)}{=} \exp\left(-2\pi\lambda \int_{r_0}^{\infty} \left(1 - \mathbb{E}_{|h|^2}\left[\exp\left(jqP|h|^2 r^{-\alpha}\right)\right]\right) rdr\right) \\
&\overset{(c)}{=} \exp\left(-2\pi\lambda \int_{r_0}^{\infty} \left(1 - \phi_{|h|^2}\left(qPr^{-\alpha}\right)\right) rdr\right)
\end{aligned}
$$

which completes the proof.

Proof of Proposition 4.4 : Let first express the joint probability with respect to the useful signal RV $\mathcal{S}$. Step (a) expresses the probability using the CDF of $\mathcal{S}$. (b) follows from the Gil-Pelaez theorem and (c) from the linearity of the expectation operator and the definition of the CF of $\mathcal{I}$.

$$
\begin{aligned}
\mathbb{F}(\theta, \theta'; r_0) &= \mathbb{P}\left[\mathrm{SIR} > \theta, \mathrm{EXPO} < \theta'\right]_{r_0} \\
&= \mathbb{P}\left[\frac{\mathcal{S}}{\mathcal{I}} > \theta, \mathcal{S} + \mathcal{I} < \theta'\right]_{r_0} \\
&= \mathbb{P}\left[\mathcal{S} > \theta\mathcal{I}, \mathcal{S} < \theta' - \mathcal{I}\right]_{r_0} \\
&\overset{(a)}{=} \mathbb{E}_{\mathcal{I}}\left[F_{\mathcal{S}}\left(\theta' - \mathcal{I}; r_0\right) - F_{\mathcal{S}}\left(\theta\mathcal{I}; r_0\right)\right]_{r_0} \\
&\overset{(b)}{=} \mathbb{E}_{\mathcal{I}}\left[\frac{1}{\pi}\int_0^{\infty} \frac{1}{q}\mathrm{Im}\left[\phi_{\mathcal{S}}(q)\left(\exp\left(-jq\theta\mathcal{I}\right) - \exp\left(-jq\theta'\right)\exp\left(jq\mathcal{I}\right)\right)\right] dq\right]_{r_0} \\
&\overset{(c)}{=} \frac{1}{\pi}\int_0^{\infty} \frac{1}{q}\mathrm{Im}\left[\phi_{\mathcal{S}}(q; r_0)\left[\phi_{\mathcal{I}}(-q\theta; r_0) - \exp\left(-jq\theta'\right)\phi_{\mathcal{I}}(q; r_0)\right]\right] dq
\end{aligned}
$$

which completes the proof.

Proof of Proposition 4.6 : *This proof is proposed in* [20]. Let denote n as the index of the tier that serves the typical user and R_k a RV expressing the distance from the nearest BS in the k^{th}-tier to the origin (notice the difference with the RV $R_{0,k}$ that applies to the serving BS).
From the Proposition 2.2, the PDF $f_{R_k}(r)$ of R_k is:

$$
f_{R_k}(r) = 2\pi\lambda_k r e^{-\pi\lambda_k r^2}, \quad r > 0.
$$

The per-tier association probability is derived as follows:

$$\begin{aligned}
\mathcal{A}_k &= \mathbb{P}\left[n = k\right] \\
&\overset{(a)}{=} \mathbb{E}_{R_k}\left[\mathbb{P}\left[P_k R_k^{-\alpha_k} > \max_{i, i\neq k} P_i R_i^{-\alpha_i}\right]\right] \\
&\overset{(b)}{=} \mathbb{E}_{R_k}\left[\prod_{i=1, i\neq k}^{K} \mathbb{P}\left[P_k R_k^{-\alpha_k} > P_i R_i^{-\alpha_i}\right]\right] \\
&= \mathbb{E}_{R_k}\left[\prod_{i=1, i\neq k}^{K} \mathbb{P}\left[R_i > \left(\frac{P_i}{P_k}\right)^{1/\alpha_i} R_k^{\alpha_k/\alpha_i}\right]\right] \\
&= \int_0^\infty \prod_{i=1, i\neq k}^{K} \mathbb{P}\left[R_i > \left(\frac{P_i}{P_k}\right)^{1/\alpha_i} r^{\alpha_k/\alpha_i}\right] f_{R_k}(r) dr
\end{aligned} \tag{A.4}$$

Step (a) follows from the expression 4.15 and (b) from the independence of the tiers. From Proposition 2.1,

$$\mathbb{P}\left[R_i > \left(\frac{P_i}{P_k}\right)^{1/\alpha_i} r^{\alpha_k/\alpha_i}\right] = \exp\left(-\pi\lambda_i \left(\frac{P_i}{P_k}\right)^{2/\alpha_i} r^{2\alpha_k/\alpha_i}\right) \tag{A.5}$$

Substituting A.5 into A.4, the per-tier association probability is:

$$\mathcal{A}_k = 2\pi\lambda_k \int_0^\infty r \exp\left(-\pi \sum_{i=1}^{K} \lambda_i \left(\frac{P_i}{P_k}\right)^{2/\alpha_j} r^{2\alpha_k/\alpha_i}\right) dr$$

If $\{\alpha_i\} = \alpha$ for all $i \in \{1, ..., K\}$, then this gives:

$$\mathcal{A}_k = 2\pi\lambda_k \int_0^\infty r \exp\left(-\pi \sum_{i=1}^{K} \lambda_i \left(\frac{P_i}{P_k}\right)^{2/\alpha} r^2\right) dr$$

Employing the change of variables $r^2 = t$ and solving the analytical integration gives:

$$\mathcal{A}_k = \frac{\lambda_k}{\sum_{i=1}^{K} \lambda_i P_i^{2/\alpha}}$$

which completes the proof.

Proof of Proposition 4.7 : *This proof is proposed in* [20]. Let denote n as the index of the tier that serves the typical user and R_k a RV expressing the distance

from the nearest BS in the k^{th}-tier to the origin.
Let first derive the expression of the CCDF $1 - F_{R_{0,k}}(r)$:

$$\begin{aligned} 1 - F_{R_{0,k}}(r) &= \mathbb{P}\left[R_k > r | n = k\right] \\ &= \frac{\mathbb{P}\left[R_k > r, n = k\right]}{\mathbb{P}\left[n = k\right]} \end{aligned} \tag{A.6}$$

The expression $\mathbb{P}[n = k]$ is given in Proposition 4.6.

$$\begin{aligned} \mathbb{P}\left[R_k > r, n = k\right] &= \mathbb{P}\left[R_k > r, P_k R_k^{-\alpha_k} > \max_{i, i \neq k} P_i R_i^{-\alpha_i}\right] \\ &= \int_r^\infty \prod_{i=1, i\neq k}^{K} \mathbb{P}\left[R_i > \left(\frac{P_i}{P_k}\right)^{1/\alpha_i} r'^{\alpha_k/\alpha_i}\right] f_{R_k}(r') dr' \\ &\overset{(a)}{=} \int_r^\infty \prod_{i=1, i\neq k}^{K} \exp\left(-\pi\lambda_i \left(\frac{P_i}{P_k}\right)^{2/\alpha_i} r'^{2\alpha_k/\alpha_i}\right) f_{R_k}(r') dr' \end{aligned} \tag{A.7}$$

Step (a) follows from A.5. Substituting A.7 into A.6,

$$F_{R_{0,k}}(r) = 1 - \frac{2\pi\lambda_k}{\mathcal{A}_k} \int_r^\infty r' \exp\left(-\pi \sum_{i=1}^{K} \lambda_i \left(\frac{P_i}{P_k}\right)^{2/\alpha_j} r'^{2\alpha_k/\alpha_j}\right) dr'$$

The PDF of $R_{0,k}$ is derived as follows :

$$\begin{aligned} f_{R_{0,k}}(r) &= \frac{dF_{R_{0,k}}(r)}{dr} \\ &= \frac{2\pi\lambda_k}{\mathcal{A}_k} r \exp\left(-\pi \sum_{i=1}^{K} \lambda_i \left(\frac{P_i}{P_k}\right)^{2/\alpha_i} r^{2\alpha_k/\alpha_i}\right), \quad r > 0 \end{aligned}$$

which completes the proof.

Proof of Proposition 4.9 : The total interference $\mathcal{I}$ is the sum of the interferences $\mathcal{I}_i$ of each tier. Step (a) follows from the independence of the tiers and (b) from the definition of the interfering signal CF.

$$\begin{aligned} \phi_{\mathcal{I}}(q; k, r_{0,k}) &= \mathbb{E}_{\mathcal{I}}\left[\exp\left(jq \sum_{i=1}^{K} \mathcal{I}_i\right)\right]_{k, r_{0,k}} \\ &\overset{(a)}{=} \prod_{i=1}^{K} \mathbb{E}_{\mathcal{I}_i}\left[\exp\left(jq\mathcal{I}_i\right)\right]_{k, r_{0,k}} \\ &\overset{(b)}{=} \prod_{i=1}^{K} \phi_{\mathcal{I}_i}(q; k, r_{0,k}) \end{aligned}$$

which completes the proof. Substituting the interference boundary $r_{\mathcal{I}_i}$ into (4.7) leads to equation (4.24).

Proof of Proposition 4.13 : *This proof is proposed in [1].* Substituting (3.16) into (4.7), the expression of the interfering signal CF for a Rayleigh fading can be derived. [1] proposes a change of variable $x = \frac{r}{(-jqP)^{1/\alpha}}$ to solve the analytical integration using the definition of the Gauss Hypergeometric function.

$$\begin{aligned}\phi_{\mathcal{I}}(q; r_0) &= \exp\left(-2\pi\lambda \int_{r_0}^{\infty}\left(1 - \frac{1}{1 - jqPr^{-\alpha}}\right) rdr\right) \\ &= \exp\left(-2\pi\lambda(-jqP)^{2/\alpha} \int_{\frac{r_0}{(-jqP)^{1/\alpha}}}^{\infty}\left(\frac{x}{x^{\alpha}+1}\right) dx\right) \\ &= \exp\left(\frac{jq2\pi\lambda P r_0^{2-\alpha}}{\alpha - 2}\, {}_2F_1\left(1, 1 - \frac{2}{\alpha}; 2 - \frac{2}{\alpha}; \frac{jq}{Pr_0^{\alpha}}\right)\right)\end{aligned}$$

which completes the proof. Substituting the interference boundary $r_{\mathcal{I}_i}$ into (4.34) leads to equation (4.35).

Proof of Proposition 5.1 : *This proof is proposed in [19].* The CP in a KTN for a PAR can be derived as follows:

$$\begin{aligned}\mathbb{P}_{\text{cv}} &= \mathbb{P}\left[\bigcup_{r_{i,k}\in\mathbf{\Phi_k},\, k\in 1,\dots,K} \text{SIR}(r_{i,k}) > \theta\right] \\ &= \mathbb{E}_{\mathbf{\Phi},|h|}\left[\mathbf{1}\left(\bigcup_{r_{i,k}\in\mathbf{\Phi_k},\, k\in 1,\dots,K} \text{SIR}(r_{i,k}) > \theta\right)\right] \\ &\overset{(a)}{=} \sum_{k=1}^{K} \sum_{x_{i,k}\in\mathbf{\Phi}_k} \mathbb{E}_{\mathbf{\Phi},|h|}\left[\mathbf{1}\left(\text{SIR}(r_{i,k}) > \theta\right)\right] \\ &\overset{(b)}{=} \sum_{k=1}^{K} 2\pi\lambda_k \int_0^{\infty} \mathbb{P}\left[\frac{P_k|h|^2 r_{i,k}^{-\alpha}}{\mathcal{I}_{x_{i,k}}} > \theta\right] r_{i,k} dr_{i,k} \\ &\overset{(c)}{=} \sum_{k=1}^{K} 2\pi\lambda_k \int_0^{\infty} \mathcal{L}_{\mathcal{I}_{x_{i,k}}}\left(\frac{\theta r_{i,k}^{\alpha}}{P_k}\right) r_{i,k} dr_{i,k}\end{aligned} \tag{A.8}$$

Step (a) follows from Lemma 2.1 under the assumption that $\theta > 1$ and from the linearity of the expectation operator, (b) follows from the Campbell Theorem and (c) follows from the Rayleigh fading and definition of the LT. $\mathcal{L}_{\mathcal{I}_{x_{i,k}}}(\cdot)$ is the LT of the interference when the user is served by the BS $x_{i,k}$. By the stationary of the HPPP, the interference does not depend on the the location of the serving BS. Therefore, $\mathcal{L}_{\mathcal{I}_{x_{i,k}}}$ is denoted by $\mathcal{L}_{\mathcal{I}}$. Unlike the proof of Proposition 4.3, the interference is defined over all the HPPP due to the impossibility of defining interference boundaries. From the independence between the tiers and the PGFL,

$$\begin{aligned}\mathcal{L}_{\mathcal{I}}(s) &\overset{(a)}{=} \prod_{j=1}^{K} \exp\left(2\pi\lambda_j \int_0^\infty \left(1 - \frac{1}{1 + sP_j r^{-\alpha}}\right) r dr\right) \\ &\overset{(b)}{=} \exp\left(-s^{2/\alpha} C(\alpha) \sum_{j=1}^{K} \lambda_j P_j^{2/\alpha}\right)\end{aligned} \tag{A.9}$$

where $C(\alpha) = \frac{2\pi^2}{\sin\left(\frac{2\pi}{\alpha}\right)\alpha}$. Step (a) follows the proof of Proposition 4.3 and Definition 3.1, and (b) from properties of the Gamma function [19]. Substituting A.9 into A.8 and solving the analytical integration, the CP is given by:

$$\mathbb{P}_{\text{cv}} = \frac{\pi}{C(\alpha)\theta^{2/\alpha}}$$

which completes the proof.

Proof of Proposition 5.2 : The JPCE in a KTN under the assumption of high SIR and a PAR can be derived as follows:

$$\begin{aligned}\mathbb{F}(\theta,\theta') &= \mathbb{P}\left[\bigcup_{r_{i,k}\in\mathbf{\Phi_k},\, k\in 1,\ldots,K} (\text{SIR}(r_{i,k}) > \theta, \text{EXPO}(r_{i,k}) < \theta')\right] \\ &= \mathbb{E}_{\mathbf{\Phi},|h|}\left[\mathbf{1}\left(\bigcup_{k\in 1,\ldots,K, x_k\in\Phi_k} (\text{SIR}(r_{i,k}) > \theta, \text{EXPO}(r_{i,k}) < \theta')\right)\right] \\ &\overset{(a)}{=} \sum_{k=1}^{K} \mathbb{E}_{\mathbf{\Phi}_k}\left[\sum_{r_{i,k}\in\mathbf{\Phi}_k} \mathbb{E}_{|h|}\left[\mathbf{1}\left(\text{SIR}(r_{i,k}) > \theta, \text{EXPO}(r_{i,k}) < \theta'\right)\right]\right] \\ &\overset{(b)}{=} \sum_{k=1}^{K} 2\pi\lambda_k \int_0^\infty \mathbb{P}\left[\frac{P_k|h|^2 r_{i,k}^{-\alpha}}{\mathcal{I}_{x_{i,k}}} > \theta, P_k|h|^2 r_{i,k}^{-\alpha} < \theta'\right] r_{i,k} dr_{i,k} \\ &= \sum_{k=1}^{K} 2\pi\lambda_k \int_0^\infty \mathbb{P}\left[\frac{\mathcal{I}_{r_{i,k}}\theta r_{i,k}^{\alpha}}{P_k} < |h|^2 < \frac{\theta' r_{i,k}^{\alpha}}{P_k}\right] r_{i,k} dr_{i,k} \\ &\overset{(c)}{=} \sum_{k=1}^{K} 2\pi\lambda_k \int_0^\infty \left[F_{|h|^2}\left(\frac{\theta' r_{i,k}^{\alpha}}{P_k}\right) - \mathbb{E}_{\mathcal{I}_{r_{i,k}}}\left[F_{|h|^2}\left(\frac{\mathcal{I}_{r_{i,k}}\theta r_{i,k}^{\alpha}}{P_k}\right)\right]\right] r_{i,k} i dr_{i,k} \\ &\overset{(d)}{=} \sum_{i=k}^{K} 2\pi\lambda_k \int_0^\infty \left[\mathbb{E}_{\mathcal{I}_{r_{i,k}}}\left[\exp\left(-\frac{\mathcal{I}_{r_{i,k}}\theta r_{i,k}^{\alpha}}{P_k}\right)\right] - \exp\left(-\frac{\theta' r_{i,k}^{\alpha}}{P_k}\right)\right] r_{i,k} i dr_{i,k} \\ &\overset{(e)}{=} \sum_{k=1}^{K} 2\pi\lambda_k \int_0^\infty \left[\mathcal{L}_{\mathcal{I}_{r_{i,k}}}\left(\frac{\theta r_{i,k}^{\alpha}}{P_k}\right) - \exp\left(-\frac{\theta' r_{i,k}^{\alpha}}{P_k}\right)\right] r_{i,k} dr_{i,k}\end{aligned} \tag{A.10}$$

Step (a) follows from Lemma 2.1 under the assumption that $\theta > 1$ and from the linearity of the expectation operator, (b) follows from the Campbell Theorem, (c) follows from the definition of the CDF, (d) from the Rayleigh fading and (e) from the definition of the LT.

Following the proof of Proposition 5.1 and from [19], the expression of the LT of the interference is defined as follows:

$$\mathcal{L}_{\mathcal{I}_{r_{i,k}}}(s) = \mathcal{L}_{\mathcal{I}}(s) = \exp\left(-s^{2/\alpha} C(\alpha) \sum_{j=1}^{K} \lambda_j P_j^{2/\alpha}\right) \tag{A.11}$$

Substituting A.11 into A.10 and by solving the analytical integration, the joint probability is given by:

$$\mathbb{F}(\theta, \theta') = \frac{\pi}{C(\alpha)\theta^{2/\alpha}} - \frac{\sum_{k=1}^{K} 2\pi\lambda_k P_k^{2/\alpha}\Gamma(\frac{2}{\alpha})}{\alpha\theta'^{2/\alpha}}$$

which completes the proof.

Proof of Proposition 5.3 : *This proof is proposed in [7].* Let σ denote the average number of BSs providing a sufficiently high power, as the following condition expresses:

$$P_k|h|^2 r^{-\alpha} > \delta \quad \forall\, k \in 1, ..., K \tag{A.12}$$

$$\begin{aligned}
\sigma &= \mathbb{E}_{\mathbf{\Phi},|h|}\left[\bigcup_{r_{i,k}\in\mathbf{\Phi_k},\, k\in 1,\ldots,K} \mathbf{1}\left(P_k|h|^2 r_{i,k}^{-\alpha} > \delta\right)\right] \\
&\overset{(a)}{=} \sum_{k=1}^{K} 2\pi\lambda_k \int_0^\infty \mathbb{P}\left[|h|^2 > \frac{\delta r_{i,k}^{\alpha}}{P_k}\right] r_{i,k} dr_{i,k} \\
&\overset{(b)}{=} \sum_{k=1}^{K} 2\pi\lambda_k \int_0^\infty \exp\left(-\frac{\delta r_{i,k}^{\alpha}}{P_k}\right) r_{i,k} dr_{i,k} \\
&\overset{(c)}{=} \frac{2\pi}{\alpha} \sum_{k=1}^{K} \lambda_k \left(\frac{P_k}{\theta'}\right)^{2/\alpha} \Gamma(\frac{2}{\alpha})
\end{aligned} \tag{A.13}$$

Step (a) follows from the linearity of the expectation operator and the Campbell Theorem, (b) follows from Rayleigh fading and (c) from properties of the Gamma function.

From the Void Probability of a PPP:

$$\mathbb{P}\left[\max_{r_{i,k}\in\mathbf{\Phi_k},\, k\in 1,\ldots,K} P_k|h|^2 r_{i,k}^{-\alpha} < \delta\right] = \exp(-\sigma) \tag{A.14}$$

Substituting A.14 and A.13 into the constraint formulation, the following inequality is obtained:

$$\frac{2\pi}{\alpha}\sum_{k=1}^{K}\lambda_k\left(\frac{P_k}{\delta}\right)^{2/\alpha}\Gamma(\frac{2}{\alpha}) > \log\frac{1}{\epsilon}$$

which completes the proof.

Proof of Proposition 6.1 : The proof is proposed for the single slope function.

$$\begin{aligned}\mathbb{P}_{P_R} &= \mathbb{P}\left[Pr^{-\alpha}|h|^2 > a\right]\\ &= \mathbb{P}\left[|h|^2 > a\frac{r^\alpha}{P}\right]\\ &\overset{(a)}{=} \int_0^\infty \exp(-\frac{r^\alpha}{P})f_R(r)dr\end{aligned} \tag{A.15}$$

Step (a) follows from Rayleigh fading. By substituting (2.3) into expression A.15, the proof is completed. For the dual slope function, the integration is split into two parts.

Appendix B

Optimization Problem

B.1 Optimization Problem 2': Tier Transmission Power

B.1.1 2-tiers Network - Analytical Solution

Let us formulate a first optimization on the powers and analysed the solution with respect to the densities.

Optimization problem 2' (**P2'**) follows the same formulation as **P2**.

Definition B.1 (P2' - 2-tiers Network)

$$\max_{P_1,P_2} \frac{C(\alpha_2,\theta)\lambda_2 P_2^{2/\alpha_2}}{\lambda_1 P_1^{2/\alpha_2} + \lambda_2 P_2^{2/\alpha_2}} - D(\alpha_2,\theta')\lambda_2 P_2^{2/\alpha_2}$$

$$\begin{aligned}
\text{such that} \quad & c_{1,1}: && \lambda_1 P_1^{2/\alpha_1} > \epsilon_1' \\
& c_{1,2}: && \lambda_2 P_2^{2/\alpha_2} > \epsilon_2' \\
& c_{2,1}: && \lambda_1 P_1^{2/\alpha_1}\left(C(\alpha_1,\theta)-\eta_1\right) - \lambda_2 P_2^{2/\alpha_1}\eta_1 > 0 \\
& c_{3,1}: && \lambda_1 P_1^{2/\alpha_1} < \epsilon_{\theta',1}' \\
& c_{4,i}: && \lambda_i \geq 0, \quad \forall i \in \{1,2\}
\end{aligned}$$

Let $\mathcal{R}$ denote the feasible region of **P2'**:

$$\mathcal{R} = \Big\{(P_1, P_2) \in \mathbb{R}_+^2 | \lambda_1 P_1^{2/\alpha_1} > \epsilon_1', \lambda_2 P_2^{2/\alpha_2} > \epsilon_2',$$
$$\lambda_1 P_1^{2/\alpha_1} (C(\alpha_1, \theta) - \eta_1) - \lambda_2 P_2^{2/\alpha_1} \eta_1 > 0, \tag{B.1}$$
$$\lambda_1 P_1^{2/\alpha_1} < \epsilon_{\theta',1}' \Big\}$$

The feasible region is illustrated Figure B.1. As mentioned in chapter 6, only the first configuration is considered.

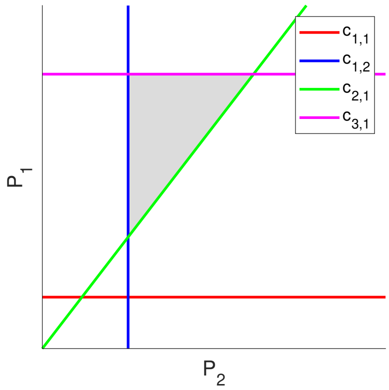

Figure B.1: **P2'** - Feasible Region

The framework used to derive the optimal solutions is similar to **P2**. The CP can be expressed as a function of the ratio $\frac{P_2}{P_1}$. Hence, the set of optimal solutions that maximizes the first term is expressed as follows:

$$(P_1^*, P_2^*) = \underset{(P_1,P_2)\in\mathcal{R}}{\arg\max} \frac{P_2}{P_1}$$

and for the second term:

$$(P_1^*, P_2^*) = \underset{(P_1,P_2)\in\mathcal{R}}{\arg\min}\, P_2$$

Therefore, the optimal solution is the intersection $(c_{1,2}, c_{2,1})$.

Proposition B.1 (P2' - Analytical Solution (P_1^*, P_2^*))

The optimal solution of **P2'** in the first configuration is given by:

$$(P_1^*, P_2^*) = \left(C(\alpha_1, \theta, \eta_1)^{-\frac{\alpha_1}{2}} \left(\frac{\lambda_2}{\lambda_1}\right)^{\frac{\alpha_1}{2}} \left(\frac{\epsilon_2'}{\lambda_2}\right)^{\frac{\alpha_2}{2}}, \left(\frac{\epsilon_2'}{\lambda_2}\right)^{\frac{\alpha_2}{2}} \right) \tag{B.2}$$

Optimization Problem 2.1': Tier Densities

At the optimal solution, the JPCE in the second tier depends on the ratio $\frac{\lambda_2}{\lambda_1}$.

Proposition B.2 ($\mathcal{F}(P_1^*, P_2^*; \theta, \theta')$)

The objective function of **P2'** evaluated at (B.2) is given by:

$$\mathcal{F}(P_1^*, P_2^*; \theta, \theta') = \frac{C(\alpha_2, \theta)}{C(\alpha_1, \theta, \eta_1)^{-\alpha_1/\alpha_2} \left(\frac{\lambda_2}{\lambda_1}\right)^{\alpha_1/\alpha_2 - 1} + 1} - D(\alpha_2, \theta')\epsilon_2' \tag{B.3}$$

The optimization on the tier transmission powers leads to a second optimization on the densities. Hence, let us formulate optimization problem 2.1' (**P2.1'**).

Definition B.2 (P2.1' - 2-tiers Network)

$$\max_{\{\lambda_i\}_{i=1}^2} \frac{C(\alpha_2, \theta)}{C(\alpha, \theta, \eta_1)^{\frac{\alpha_2}{\alpha_1}} \left(\frac{\lambda_2}{\lambda_1}\right)^{\frac{\alpha_1}{\alpha_2} - 1} + 1} - D(\alpha_2, \theta')\epsilon_2'$$

$$\begin{aligned}
\text{such that} \quad & c_{1,1}: \quad \lambda_1 P_1^{*2/\alpha_1} > \epsilon_1' \\
& c_{1,2}: \quad \lambda_2 P_2^{*2/\alpha_2} > \epsilon_2' \\
& c_{2,1}: \quad \lambda_1 P_1^{*2/\alpha_1} \left(C(\alpha_1, \theta) - \eta_1\right) - \lambda_2 P_2^{*2/\alpha_1} \eta_1 > 0 \\
& c_{3,1}: \quad \lambda_1 P_1^{*2/\alpha_1} < \epsilon_{\theta',1}' \\
& c_4: \quad \lambda_2^{1 - \frac{\alpha_2}{\alpha_1}} > \frac{\epsilon_1'}{\epsilon_2'^{\frac{\alpha_2}{\alpha_1}}} C(\alpha_1, \theta, \eta_1) \\
& c_{5,i}: \quad \lambda_i \geq 0, \quad \forall i \in \{1, 2\}
\end{aligned}$$

The constraint c_4 is the condition to be in the first configuration (obtained from (6.22)). By substituting (B.2) in constraints expressions, the feasible region, denoted by $\mathcal{R}$, is defined as follows:

$$\begin{aligned}
\mathcal{R} = \Big\{ & (\lambda_1, \lambda_2) \in \mathbb{R}_+^2 | \lambda_2^{1 - \frac{\alpha_2}{\alpha_1}} > \frac{\epsilon_1'}{\epsilon_2'^{\frac{\alpha_2}{\alpha_1}}} C(\alpha_1, \theta, \eta_1), \\
& \lambda_2^{1 - \frac{\alpha_2}{\alpha_1}} < \frac{\epsilon_{1,\theta'}'}{\epsilon_2'^{\frac{\alpha_2}{\alpha_1}}} C(\alpha_1, \theta, \eta_1) \Big\}
\end{aligned} \tag{B.4}$$

Figure B.2 shows a visualization of the feasible region.

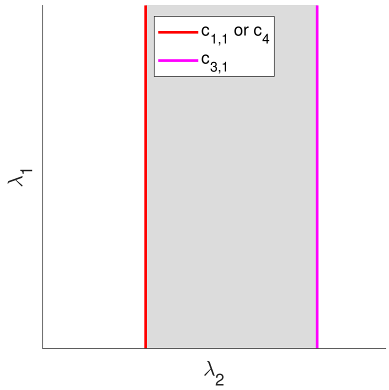

Figure B.2: **P2.1'** - Feasible Region

Assuming $\alpha_2 > \alpha_1$, one can deduce that the optimal solution to **P2.1** is expressed as follows:

$$(\lambda_1^*, \lambda_2^*) = \arg\max_{(\lambda_1,\lambda_2)\in\mathcal{R}} \frac{\lambda_2}{\lambda_1} \tag{B.5}$$

Bibliography

[1] Hesham ElSawy, Ahmed Sultan-Salem, Mohamed-Slim Alouini and Moe Z. Win, "Modeling and Analysis of Cellular Networks Using Stochastic Geometry: A Tutorial", *IEEE communications surveys* & tutorials, Vol. 19, No. 1, p.167 - 203, First Quarter 2017.

[2] Koustubh Sharma, "Comparison of energy efficiency between macro and micro cells using energy saving schemes", *Master's Thesis*, 2017.

[3] V. Chandrasekhar, J.G. Andrews, "Femtocell Networks: A Survey", *IEEE Communications Magazine*, Vol. 46, No. 9, p.59 - 67, September 2008.

[4] Matti Latva-aho, "Infotech Oulu Annual Report 2014 - Radio Access Technologies (RAT)", `https://www.oulu.fi/infotech/annual_report/2014/rat`, 9^{th} April 2015.

[5] Marco Di Renzo, Alessio Zappone, Thanh Tu Lam and Mérouane Debbah, "System-Level Modeling and Optimization of the Energy Efficiency in Cellular Networks - A Stochastic Geometry Framework", *IEEE Transactions on wireless communications* Vol. 14, No. 4, p.2539 - 2556, April 2018.

[6] Yanzan Sun , Li Xu , Yating Wu , Tao Wang , Weidong Fang , Lianhai Shan and Yong Fang, "Energy Efficient Small Cell Density Optimization Based on Stochastic Geometry in Ultra-Dense HetNets", *9th IEEE International Conference on Communication Software and Networks*, 2017.

[7] Ran Cai, Wei Zhang and P. C. Ching, "Cost-Efficient Optimization of Base Station Densities for Multitier Heterogeneous Cellular Networks", *IEEE Transactions on wireless communications*, Vol, 15, No, 3, p.2381 - 2393, March 2016.

[8] Marco Di Renzo, "Intro to Stochastic Geometry Point Process", *Course on Random Graphs and Wireless Commun. Netwrok*, 2016.

[9] Dennis D.Wackerly, William Mendenhall III and Richard L. Scheaffer, "Mathematical Statistics with Applications", *Seventh edition, Brooks/Cole, Cengage Learning*, 2014.

[10] François DE Saint Moulin, "Stochastic Geometry-based Modelling of Wireless Communication Networks, UAV-based Networks" Ecole polytechnique de Louvain, Université catholique de Louvain, 2020. Prom. : Claude Oestges ; Luc Vandendorpe

[11] M. Gevers and L. Vandendrope, "INMA 1731 : Processus stochastiques, estimation et prédiction", *LINMA 1731 - Stochastic Process*, Ecole Polytechnique de Louvain-La-Neuve.

[12] "JPL's Wireless Communication Reference Website", `http://www.wirelesscommunication.nl/reference/chaptr03/propmain.htm`, 1999.

[13] Arif Sari, Ahmed Alzub, "Path Loss Algorithms for Data Resilience in Wireless Body Area Networks for Healthcare Framework", *Security and Resilience in Intelligent Data-Centric Systems and Communication Networks*, 2018.

[14] Shu Sun, Timothy A. Thomas, Theodore S. Rappaport, Huan Nguyen, Istvànd Z. Kovàcs, and Ignacio Rodriguez, "Path Loss, Shadow Fading, and Line-Of-Sight Probability Models for 5G Urban Macro-Cellular Scenarios", *IEEE Globecom Workshops*, December 2015.

[15] Claude Oestges, "Mobile Propagation Channels 1 – Path Loss and Shadowing", *LELEC2796 - Wireless Communications*, Ecole Polytechnique de Louvain-La-Neuve.

[16] Xianghao Yu, Jun Zhang, Martin Haenggi and Khaled B. Letaief, "Coverage Analysis for Millimeter Wave Networks: The Impact of Directional Antenna Arrays", *IEEE journal on selected areas in communications*, Vol. 35, No. 7, p.1498 - 1512, July 2017.

[17] Dr. Jacques Vanderstraeten, Dr. Marion Crasson, Dr. Ir. Benoît Stockbroeckx, "Les champs électromagnétiques et la santé". *Brochure*, 2008.

[18] International Telecommunication Union, "Characteristics of terrestrial IMT-Advanced systems for frequency sharing/ interference analyses", Report ITU-R M.2292-0, December 2013.

[19] Harpreet S. Dhillon, Radha Krishna Ganti, Franc¸ois Baccelli and Jeffrey G. Andrews, "Modeling and Analysis of K-Tier Downlink Heterogeneous Cellular Networks", *IEEE journal on selected areas in communications*, Vol. 30, No. 3, p.550 - 560, April 2012.

[20] Han-Shin Jo, Young Jin Sang and Ping Xia and Jeffrey G. Andrews, "Heterogeneous Cellular Networks with Flexible Cell Association: A Comprehensive Downlink SINR Analysis", *IEEE Transactions on wireless communications*, Vol. 11, No. 10, p.3484 - 3495, October 2012.

[21] Hesham ElSawy and Ekram Hossaim, "On Stochastic Geometry Modeling of Cellular Uplink Transmission With Truncated Channel Inversion Power Control", *IEEE Transactions on wireless communications*, Vol. 13, No. 8, p.4454 - 4469, August 2014.

[22] Hesham ElSawy, Ekram Hossain, and Martin Haenggi, "Stochastic Geometry for Modeling, Analysis, and Design of Multi-Tier and Cognitive Cellular Wireless Networks: A Survey", *IEEE Communications surveys* & *Tutorials* Vol. 15, No. 3, p.996 - 1019, Third Quarter 2013.

UNIVERSITÉ CATHOLIQUE DE LOUVAIN
École polytechnique de Louvain
Rue Archimède, 1 bte L6.11.01, 1348 Louvain-la-Neuve, Belgique | **www.uclouvain.be/epl**